ZrO2 addition in soda-lime aluminoborosilicate glasses containing rare earths: Impact on the network structure

Arnaud Quintas, Daniel Caurant, Odile Majérus, Pascal Loiseau, Thibault Charpentier, Jean-Luc Dussossoy

ZrO_2 addition in soda-lime aluminoborosilicate glasses containing rare earths : Impact on the network structure

Arnaud Quintas [a], Daniel Caurant [b,*], Odile Majérus [b], Pascal Loiseau [b], Thibault Charpentier [c], Jean-Luc Dussossoy [d]

[a] *Laboratoire Commun Vitrification AREVA-CEA, 30207 Bagnols-sur-Cèze, France*

[b] *Chimie ParisTech, PSL Research University, CNRS, Institut de Recherche de Chimie Paris (IRCP), 75005 Paris, France*

[c] *NIMBE, CEA, CNRS, Université Paris-Saclay, CEA Saclay, 91191 Gif-sur-Yvette cedex, France*

[d] *CEA, DEN, DE2D/SEVT – Marcoule, F-30207 Bagnols sur Cèze, France*

Abstract

The influence of increasing ZrO_2 content on the structural features of a rare earths (RE = Nd, La) bearing soda-lime aluminoborosilicate glass was investigated through a multi-spectroscopic approach (Raman, Zr-EXAFS, ^{29}Si, ^{11}B, ^{27}Al and ^{23}Na MAS NMR). Particular attention was paid to the modifications occurring in the glassy network and on the distribution of Na^+ and Ca^{2+} ions. Zr^{4+} ions were shown to be located in $(ZrO_6)^{2-}$ sites, connected to the silicate network, and preferentially charge compensated by Na^+ ions. A favorable competition of Zr^{4+} ions against RE^{3+} ions and $(BO_4)^-$ entities for charge compensators was observed, but no effect was detected on the environment of $(AlO_4)^-$

* Corresponding author: E-mail address: daniel.caurant@chimie-paristech.fr (Daniel Caurant)

entities. This competition resulted in a modification of the RE^{3+} ions environment with the ZrO_2 content that may affect their solubility in the glassy network.

1. Introduction

Because of its beneficial properties on silicate glasses alteration and controlled crystallization, zirconium is an element that frequently enters into the composition of industrial glasses and glass-ceramics. For instance, ZrO_2 is known to increase the chemical durability of glasses [1,2,3] and can be used to prepare alkali-resistant glass fibers for reinforcement of cement products [4,5]. Depending on glass composition, ZrO_2 may also act as an efficient nucleating agent in silicate glasses [6,7,8,9,10]. It is also well known that ZrO_2 associated with TiO_2 induces the crystallization in the bulk of transparent lithium aluminosilicate (LAS) glass-ceramics with very low thermal expansion [11,12,13,14]. Moreover, ZrO_2 is known to lead to the crystallization of zirconolite ($CaZrTi_2O_7$) in the bulk of calcium aluminosilicate glass-ceramics that have been developed for actinides immobilization [15]. Besides, zirconium is one of the main constituent of fluorozirconate glasses that are well known for their good transmission in the visible and infrared ranges [16].

ZrO_2 is also present in borosilicate glasses used to immobilize highly radioactive nuclear wastes arising from the reprocessing of spent nuclear fuels. In these glasses, zirconium originates both from the highly radioactive waste solutions (as fission product and as fine metallic particles of zirconium alloy cladding material used to enclose the fuel in reactors and that are generated during the cutting of the cladding tubes) and from the glass frit added to the wastes for glass preparation (ZrO_2 is present in the glass frit composition to improve the nuclear glass chemical durability) [17,18]. A small fraction (≈ 10%) of all the Zr occurring in waste solutions as fission product is radioactive (^{93}Zr is

a weak β-emitter with a half-life time close to 1 500 000 years) [19] but this is not a problem because of the very low solubility of ZrO_2 in water and of the very low mobility of Zr^{4+} ions in geologic environment. Nevertheless, the presence of significant amount of zirconium in the final containment matrix should be considered with great interest when a good mastering of the waste form performance is required. In this frame, achievement of a comprehension of the effect of the presence of zirconium on the properties and behavior of the glass is strongly recommended. This is why extensive studies have been performed on simplified borosilicate nuclear glasses to improve the understanding of the role of ZrO_2 on their alteration mechanisms in water [2,3,20,21,22].

In order to reduce the volume of glass needed to immobilize radioactive wastes, new glass compositions able to immobilize higher concentrations of wastes than today are under development in different countries [17,23,24,25,26,27,28]. For instance, aluminoborosilicate glasses have been envisaged in France for the immobilization of the highly concentrated waste solutions that would arise from the reprocessing of high burn-up UO_2 spent fuels [17,19,23,26,27]. In previous works, we investigated the effect of composition changes (RE_2O_3 [23,29], Al_2O_3 [23] and B_2O_3 [30] contents, RE nature [31], Na/Ca ratio [32], alkali and alkaline earth nature [33]) on the structure and crystallization tendency of a simplified 7-oxides version of such glasses (glass Zr1, Table 1). In this RE-rich soda-lime aluminoborosilicate glass, RE simulates all the rare earths and actinides occurring in the wastes. We focussed our studies on the environment of RE^{3+} ions, on the structure of the glassy network and on the crystallization tendency during cooling of the melt of a RE silicate apatite phase ($Ca_2RE_8(SiO_4)_6O_2$) that may incorporate minor actinides in its structure [34,35].

The aim of the present study was to complete these previous works by focusing the investigation on the structural role of zirconium in this RE-rich soda-lime

aluminoborosilicate glass system. For this, we studied the effect of zirconia content (from 0 to 5.7 mol%) on the glassy network structure. The resulting effect of composition changes on the glass structure at an atomic scale, as regards to the glassy network arrangement and cation species distribution was investigated using a multi-spectroscopic approach (NMR, EXAFS and Raman spectroscopies). Special attention was paid to the local environment of Zr^{4+} ions. To clarify the impact of ZrO_2 addition on the structure of the 7-oxides glass, a series of ternary sodium silicate glasses with increasing ZrO_2 content was also prepared and studied (NMR, Raman). To complete this work, the effect of zirconia content on RE^{3+} (RE = Nd) environment and glass crystallization tendency (RE-apatite crystallization) has also been investigated and is presented in another paper [36].

2. Structural role of Zr^{4+} ions in silicate glasses and its impact on glass properties

In alkali-rich silicate and borosilicate glasses (i.e. in glasses with high non-bridging oxygen atoms (NBOs) content), Zr^{4+} ions are 6-fold coordinated (CN=6) and $(ZrO_6)^{2-}$ octahedra share corners with SiO_4 tetrahedra as shown by EXAFS spectroscopy and bond valence - bond length considerations [37,38 ,39,40,41,42,43,44]. The existence of Zr-O-Si bonds in these glasses was also shown directly by ^{17}O MQMAS NMR experiments [45]. Nevertheless, a local charge compensation (brought for instance by alkali or alkaline-earth ions) is needed to stabilize the negative charge excess of $(ZrO_6)^{2-}$ octahedra. Because of the strong bonding between Zr and the silicate network and of the increasing presence of alkali or alkaline-earth ions close to the oxygen atoms connecting Zr and Si when the ZrO_2 content is increased, ZrO_2 can be considered as a reticulating oxide in such glasses. Moreover, ^{11}B MAS NMR results obtained on soda-lime borosilicate glasses containing Zr showed that $(ZrO_6)^{2-}$ octahedra are charge compensated at the expense of a part of $(BO_4)^-$ tetrahedral units (a drop of the proportion of $(BO_4)^-$ units

was observed when ZrO_2 was added to the glass composition) [45,46]. The same MAS NMR study suggested that both $(ZrO_6)^{2-}$ and $(BO_4)^-$ entities were preferentially charge compensated by Na^+ rather than by Ca^{2+} ions [46]. A more recent Zr $L_{2,3}$-edge and K-edge EXAFS study performed on soda lime borosilicate glasses with increasing ZrO_2 content suggests that $(ZrO_6)^{2-}$ octahedra are charge compensated by $2Na^+$ and have 4Si and 2B second neighbors, with mainly 4-coordinated boron [44]. According to aqueous alteration tests and Monte Carlo modelling methods to simulate the alteration of soda-lime borosilicate glasses, the effect of zirconium on glass chemical durability appeared rather complex [2,47,48]: the presence of Zr-O-Si bonds in the glass structure would improve the glass alteration resistance by limiting the dissolution of the neighboring Si atoms (which is favorable in terms of alteration kinetics) but the presence of increasing zirconium content in glass would inhibit the recondensation of silicon atoms in the gel layer formed during alteration thus preventing the closure of the gel porosity. Adding ZrO_2 to soda-lime borosilicate glasses would thus increase the surface area of the gel layer (thus decreasing its protective properties) and would thus increase the amount of glass altered on the long term. In accordance with these studies, ^{17}O MQMAS NMR results suggested that the octahedral coordination of zirconium remained unchanged in the alteration gel recovered after glass alteration in static mode (presence of Zr-O-Si bonds in the gel) [45]. This last result was confirmed by comparing Zr XAS spectra of Zr-bearing pristine and altered glasses in near-saturation conditions [22,48].

In more polymerized glasses - i.e. in glasses with lower non-bridging oxygen atoms (NBOs) content - such as albite glass ($6SiO_2.Al_2O_3.Na_2O$), EXAFS results suggested that a significant amount of zirconium ions would occur in 8-fold coordinated (CN=8) sites (sharing edges with SiO_4 tetrahedra as in zircon $ZrSiO_4$) but the majority of zirconium ions would occur in 6-fold coordinated sites [37]. Such an increase of the Zr

coordination (CN > 6) with silicate glass polymerization was confirmed by XANES and EXAFS results obtained on glasses belonging to the SiO_2-Al_2O_3-MgO-ZnO-ZrO_2 system [6,7]: in such glasses Zr would be in 7-fold coordination, edge-sharing linkages with SiO_4 tetrahedra and forming bonds with other Zr polyhedra [7]. According to [6,7,49], such a high Zr coordination due to a lack of efficient local charge compensation by modifier ions, would prefigure the local organization existing in Zr-rich crystalline phases which would explain the Zr instability in these glasses during heat treatment (crystallization of ZrO_2 nano-particles [7,49]) and then its nucleating effect on glass crystallization. Nevertheless, a very recent study showed that Zr could also have a strong nucleating effect even in 6-fold coordination in a glass belonging to the SiO_2-Al_2O_3-Li_2O system due to existence of direct Zr-Zr polyhedra linkages [10].

3. Experimental procedure

3.1. Glass synthesis

Two glass series referred to as ZrxRE with RE = Nd or La and with ZrO_2 content varying from 0 to 5.69 mol% have been prepared for this study (Table 1). The composition of these 7-oxides glass series derives from that of a more complex nuclear glass studied in [23]. In all glasses of these series the total RE_2O_3 concentration was close to 3.4-3.7 mol% (15-16 wt%). The ZrxLa series was prepared as a complement of the ZrxNd series to perform NMR studies. Indeed, NMR cannot be performed on ZrxNd glasses because of the presence of a high concentration of paramagnetic species (Nd^{3+}). Nevertheless, to decrease the relaxation time during NMR experiments, a very small amount of Nd_2O_3 (0.15 mol%) was introduced in all ZrxLa glasses. The ZrxNd series was prepared to follow the evolution of the environment of Nd^{3+} ions with zirconia content by optical absorption spectroscopy (indeed, because of the lack of f electrons, La^{3+} ($4f^0$) ions

cannot be studied by this spectroscopy) and Nd-EXAFS as shown in another paper [36]. The Zr1RE glass (with 1.9 mol% ZrO_2) corresponds to the simplified version of an inactive reference waste containment glass already studied in other papers [23,32,33,50,51]. All glasses were melted from the appropriate quantities of SiO_2, H_3BO_3, Al_2O_3, Na_2CO_3, $CaCO_3$, ZrO_2, La_2O_3 and Nd_2O_3 reagent grade powders previously dried for one night (except for H_3BO_3) at 400°C or 1000°C. 50g of mixed powders were melted in air at 1300°C in Pt crucibles for 3h (heating rate at 100°C/h from room temperature to 1300°C). Then, the melt was heated for 15min at 1400°C in order to decrease its viscosity, before being poured into cold water. The glass frit obtained was then dried, ground in an agate mortar and melted again at 1300°C for 2h to ensure homogeneity. The melt was then cast in steel moulds at room temperature to form glass cylinders (14 mm diameter and 10 mm high). All ZrxRE glass samples were transparent and amorphous according to X-ray diffraction. They were analysed by Inductively Coupled Plasma Atomic Emission Spectrometry (ICP AES) and the compositions are given in Table 1. By comparison with the nominal compositions, only a relatively slight depletion in B_2O_3 (1 - 14 %) and Na_2O (4 - 6 %) - that are the most volatile oxides present in these glasses - was observed.

To complete the structural study (Raman, NMR) of the effect of ZrO_2 addition on the structure of the silicate network of the glasses of the ZrxRE series, a complementary Zrx series of simple sodium silicate glasses with increasing ZrO_2 content (0 - 10 mol%) and without RE was also prepared (Table 2). All glasses of the Zrx series were melted from the appropriate quantities (nominal compositions) of SiO_2, Na_2CO_3 and ZrO_2 reagent grade powders previously dried for one night at 400°C. 20g of mixed powders were melted at 1565°C in Pt crucibles for 2 h (heating rate at 300°C/h from room temperature to 1565°C). To increase glasses homogeneity, melts were then quenched to room

temperature, ground in an agate mortar and melted again at 1565°C for 3h before quenching again to room temperature. Zrx glasses were not annealed after quenching because they were not cut for optical absorption characterization. The higher temperature used to melt Zrx glasses (1565°C) in comparison with ZrxRE glasses (1300°C) was both due to the lack of B_2O_3 and to the higher SiO_2 and ZrO_2 amounts in glasses of the Zrx series. It is important to note that during melting at such a high temperature, a high proportion of Na_2O evaporates. Indeed, ICP AES revealed that the true Na_2O content is about 8% lower than the theoretical content for all Zrx glasses (Table 2). Nevertheless, the relative proportion of Na_2O to SiO_2 remains close to 0.17 for the three glasses and the Na_2O/ZrO_2 ratio always remains higher than 1 for Zr5 (2.36) and Zr10 (1.19) glasses (Table 2). In this paper, we will thus use the true composition taking into account Na_2O evaporation rather than the nominal one for the glasses of the Zrx series.

3.2. Characterization methods

ZrxNd glasses structural characterization was performed by Zr-EXAFS and Raman spectroscopy. Zr-EXAFS measurements (Zr1Nd and Zr3Nd glasses) were performed at 300K at Zr K-edge (17998 eV) at ANKA synchrotron (Karlsruhe, Germany), using the INE beamline. Glass samples were grounded, diluted with cellulose and pressed into pellets. Spectra were acquired in transmission mode. For each sample, 4 scans were accumulated to improve the signal to noise ratio with a k step of $0.03Å^{-1}$ and the spectra were measured up to $16Å^{-1}$ above the edge. For the analysis of the data, amplitude and phase diffusion factors were calculated with the help of FEFF8 and the simulations were carried out with the UWXAFS program. In the simulations, coordination numbers were constrained to the mean Zr-O first shell distance to satisfy the bond valence principle [42].

Raman study of ZrxNd and ZrxLa glasses was carried out on a T64000 Jobin-Yvon confocal microRaman spectrometer equipped with a CCD detector cooled by nitrogen and using the 488 nm line of a Coherent 70 Ar^+ laser as excitation source operating at approximately 2W. Raman spectra of Zrx glasses were recorded with a HORIBA Jobin-Yvon Aramis microspectrometer using a He-Cd laser as excitation source (325 nm, 30 mW). In all cases, unpolarized Raman spectra were collected at room temperature and were corrected for temperature and frequency dependency of the scattering intensity using a correction factor of the form proposed by Long [52]. A third order polynomial baseline was fitted directly to the corrected Raman spectra which were then normalized to unit total area.

MAS NMR studies were only performed on ZrxLa and Zrx glasses. ^{11}B, ^{23}Na, ^{27}Al MAS and ^{29}Si NMR experiments and spectra simulations to extract the proportion of BO_4 units and the ^{27}Al and ^{23}Na NMR mean isotropic chemical shift (δ_{iso} parameters) and mean quadrupolar coupling constant (C_Q) were performed as described in [32] with a Bruker Avance II 500 WB spectrometer (11.75 T). A Bruker CPMAS BL4 WVT (stator made of MgO to avoid the ^{11}B background signal) probe with 4 mm outside diameter ZrO_2 rotors and a spinning speed of 12.5 kHz was used. ^{11}B, ^{23}Na, ^{27}Al and ^{29}Si chemical shifts are reported in ppm relative respectively to an external sample of 1.0M aqueous boric acid at 19.6 ppm, 1.0M aqueous NaCl at 0 ppm, 1.0M aqueous $Al(NO_3)_3$ at 0 ppm and tetrakis(trimethylsilyl)silane powder characterized by two lines at -9.9 ppm and -135.3 ppm with respect to tetramethylsilane. For more details on NMR experimental conditions, see reference [32].

Glass transition temperature T_g was measured by differential thermal analysis (DTA) for all glasses of the ZrxNd and ZrxLa series. About 200 mg of glass powders

(particle size 80-125µm) were heated with a Netzsch STA409 apparatus in Pt crucibles using α-Al_2O_3 as reference material (heating rate 10°C/min).

4. Results and discussion

4.1. Physical properties of glasses

The evolution of the density of ZrxRE glasses with ZrO_2 concentration is shown in Fig. 1a. The glass density measurements have been performed at room temperature by the Archimedes'principle using distilled water as the immersion liquid (6 repeated measurements were performed for each glass). The monotonous increase of the density observed is due to the high molecular weight of ZrO_2 (123.2 g/mol). It is also the higher molecular weight of Nd_2O_3 (336.5 g/mol) in comparison with La_2O_3 (325.8 g/mol) that explains the relative position of the two curves in Fig. 1a. Knowing the composition of glasses and their density it was possible to calculate their oxygen molar volume $V_m(O)$ [32,53] that represents the packing of the glass structure (Fig. 1b). It appears that the oxygen atoms network becomes more and more compact with ZrO_2 content ($V_m(O)$ decreases). No significant effect of the nature of the RE on $V_m(O)$ was observed for the highest ZrO_2 concentrations.

A significant and progressive increase of T_g is observed with the ZrO_2 content (Fig. 1c, Table 1) that can be explained by the structural role of zirconium in glass structure (reticulating effect). Indeed, according to the results that will be presented below (Sections 4.2.1 and 4.2.2.4), the progressive introduction of ZrO_2 induces the formation of strong Zr-O-Si bonds and the moving of an increasing amount of Na^+ ions from a modifier position (close to NBOs) to a charge compensator position close to $(ZrO_6)^{2-}$ units. The increase of T_g with the nature of the RE (T_g (ZrxNd) > T_g (ZrxLa)) observed in Fig. 1c can be explained by the higher field strength of the Nd^{3+} ion in

comparison with the La^{3+} ion due to the lower size of the Nd^{3+} ion. This is in accordance with our previous results on glasses with RE varying from La to Lu [31]. A higher increase of T_g with ZrO_2 content was reported in SiO_2-Na_2O-CaO-ZrO_2 glasses [54] probably due to the presence of B_2O_3 and the decrease of the proportion of BO_4 units in our glass (see Section 4.2.2.3).

4.2. Structural investigation of glasses

4.2.1. Zirconium environment

The immediate Zr environment was investigated through EXAFS experiments. Fig. 2 reports the modulus of the Fourier transforms of the Zr K-edge k^3-weighted EXAFS function $\chi(k)$ of glasses Zr1Nd and Zr3Nd and Table 3 presents the fitting results. These data clearly show that the Zr environment remains unchanged in the first and second coordination shell while ZrO_2 content increases from 1.9 to 5.69 mol%. The results are consistent with Zr occupying a position 6-fold coordinated to oxygen in glass structure with a small radial disorder (low σ^2 values, Table 3). Attempts to simulate the second shell contribution of Zr to determine the nature of the second neighbors were done. Trying Zr as second neighbor revealed unsuccessful which precludes the existence of Zr-O-Zr linkages in our glasses for all ZrO_2 contents which is accordance with the fact that no significant change of the second shell contribution occurred with ZrO_2 content (Fig. 2). On the contrary, best results were obtained by considering Si as second neighbor (existence of Zr-O-Si linkages). Comparison of EXAFS parameters of Zr in ZrxNd glasses with those of the crystalline alkali Zr-rich silicate zektzerite ($LiNaZrSi_6O_{15}$) shows great similarity (Table 3). In zektzerite, almost regular ZrO_6 octahedra share corners with SiO_4 Q_3 units (Q_n units correspond to SiO_4 tetrahedra bonded to n SiO_4 tetrahedra) and alkali ions insured local charge compensation (see the inset in Fig. 4) [55]. In the rest of the paper, we will refer this kind of SiO_4 tetrahedra to as Q_3(Zr). In

zektzerite there is just enough alkali ions to compensate all $(ZrO_6)^{2-}$ entities and just enough SiO_2 to enable to these entities to be connected to 6 SiO_4 units (Si/Zr = 6). This result suggests that similar connectivity of Zr with the surrounding silicate network should be found in our glasses. Similar results were obtained by McKeown et al. on their Zr-rich borosilicate glasses by comparison with zektzerite EXAFS data [38]. The presence of a small fraction of B or Al as second neighbors of Zr can also be envisaged [44].

The Zr-O mean distance in ZrxNd glasses was also compared with that of various other ZrO_2-bearing silicate glass compositions. Our glasses exhibit Zr-O mean distance (2.09 Å) close to that of ZrO_2-bearing soda aluminosilicate (2.07Å) [37,39] and soda-lime aluminoborosilicate (2.08-2.09Å) [40,44] glasses. This distance is significantly lower than the Zr-O mean distance (≥ 2.14Å) in ZrO_2-bearing calcium aluminosilicate and calcium silicate glasses (G1 and G2 glasses, Table 3). In these glasses containing mainly calcium as charge compensator, the Zr-O-Si linkages are mainly or totally charge compensated by Ca^{2+} ions (as Ca^{2+} has higher field strength than Na^{+} it induces a lengthening of the Zr-O distance, probably associated to an increase in average coordination number). This comparison suggests that in ZrxNd glasses, ZrO_6 octahedra are preferentially charge compensated by Na^{+} ions rather than by Ca^{2+} ions (see the inset in Fig. 2) which is in accordance with [44,46]. Consequently, $(ZrO_6)^{2-}$ entities behave similarly to $(AlO_4)^{-}$ and $(BO_4)^{-}$ entities that are preferentially charge compensated by alkali ions (Na^{+}) rather than by alkaline-earth ions (Ca^{2+}) in aluminoborosilicate glasses [33]. This behavior can be explained by the preferential acid-base reaction of the acid oxides (Al_2O_3, B_2O_3, ZrO_2, i.e. M_xO_y oxides where $M^{(2y/x)+}$ are high field strength ions) with the most basic oxides available in the silicate melt (Na_2O). Indeed, the basicity of oxides (related to their electron donor power and oxygen polarisability) is known to

increase with decreasing the cation–O^{2-} bond strength (related to the cation electronegativity) [56] and for instance, according to the scale of Duffy and Ingram [57], alkali and alkaline earth oxides can be ranked in the following order of decreasing optical basicity Λ: $Cs_2O > K_2O > Na_2O \approx BaO > SrO > Li_2O \approx CaO > MgO$. The acid-base reaction between ZrO_2, SiO_2 and Na_2O in the silicate melt can be ideally written as: $ZrO_2 + 6Q_4 + Na_2O \rightarrow ((ZrO_6)^{2-},2Na^+)\text{-}6Q_3(Zr)$. Thus, the reaction of ZrO_2 with Na_2O both reduces the formation of NBOs (oxygen atoms belonging to Si-O-Zr bonds are not considered as a NBOs, this why ZrO_2 is considered as a reticulating agent) and affects the distribution of Na^+ ions within the glassy network.

As the molar ratio Na_2O/ZrO_2 is systematically greater than 1 for all glasses of the ZrxRE series (Table 1), the amount of Na_2O is largely sufficient to enable the incorporation of zirconium only as $(ZrO_6)^{2-}$ octahedra in glass structure. As it will be seen later, even by considering the aluminum and boron charge compensation requirements by Na^+ ions ($(AlO_4)^-$ and $(BO_4)^-$ entities), the sodium content is still sufficient to charge compensate all $(ZrO_6)^{2-}$ entities for all the glasses of the ZrxRE series. Thus, for all glasses of the series, the $(ZrO_6)^{2-}$ entities can exist as isolated species in the silicate network because they do not need to share NBOs to dissolve in the network.

4.2.2. Structure of the aluminoborosilicate glass network

The structure of the glassy network was examined with both Raman and MAS NMR (^{27}Al, ^{11}B, ^{23}Na, ^{29}Si) spectroscopies.

4.2.2.1. Raman study

Fig. 3 shows the Raman spectra of ZrxNd glasses in the 100-1600 cm^{-1} range. A very similar evolution of Raman spectra was observed with the ZrO_2 content for the glasses of the ZrxLa series (spectra not shown) which indicates that the nature of the RE

has not significant impact on the effect of zirconium addition on the silicate network structure at least for the RE of the beginning of the lanthanide series. In the low frequency range (100-800 cm^{-1}) an increasing and wide contribution attributed to the bending and stretching vibration modes of Si-O-Si bonds [58] is observed near 525 cm^{-1} whereas the intensity of the band close to 635 cm^{-1} seems to decrease when the ZrO_2 content increases (Fig. 3). A similar, narrow band around 630 cm^{-1} appears in alkali borosilicate glasses [46,59,60] and is generally attributed to the breathing mode of borosilicate rings with ^{IV}B–O–Si bonds. It has been proposed that this band was related to danburite rings composed of 2 $(BO_4)^-$ and 2 (SiO_4) tetrahedral [48,60] by comparison with the Raman spectrum of the danburite mineral [60] ($CaO.B_2O_3.2SiO_2$, showing an intense Raman peak at 615 cm^{-1}). The decrease of the "danburite-like" contribution could be explained by the decrease of the amount of boron in tetrahedral coordination [46] (see Section 4.2.2.3). The intensity of the large Si–O–Si bending band at about 525 cm^{-1} remains constant, indicating that the polymerization degree of the silicate network is hardly affected by the ZrO_2 content increase. A slight increase in intensity of the low-frequency edge (around 360 cm^{-1}) of this band may be possibly due to the contribution of Si–O–Zr bending modes. Indeed, the rising of such a contribution is put in evidence in the Raman spectra of the Zrx glass series in Fig. 7. This contribution is also observed in the spectra of reference [46].

In the high frequency range (1300-1600 cm^{-1}), the band at about 1435 cm^{-1} is assigned to the B–O stretching mode in $(BO_3)^-$ metaborate groups. This band gets broader towards the low-frequency side. It is possible that new $(BO_3)^-$ units, bonded to high-field strength second neighbours (Ca^{2+}, Nd^{3+}…), and thus experiencing a lower B-O bond strength (lower B-O stretching frequency), appear with the ZrO_2 content increase.

In Fig. 4 is detailed the 800-1250 cm^{-1} range of the Raman spectra (ZrxNd series) corresponding to the Si-O stretching modes within the SiO_4 Q_n units. For all spectra, fitting procedure was performed with four Gaussian bands associated with the stretching vibration of different Q_n units [61] (examples of fits are presented in Fig. 5 for the Zr0Nd and Zr3Nd glasses). The attribution of the bands was performed taking into account the fact that the stretching vibration of Q_{n-1} units appears at lower frequency than that of Q_n units [62]. Band positions are given in Table 4 and the evolution of their relative areas with the ZrO_2 content is reported in Fig. 6 for both ZrxNd and ZrxLa series. It clearly appears that the total replacement of Nd by La in glass composition has not significant effect on both bands position and relative intensity when the ZrO_2 content increases (Table 4, Fig. 6). In this energy range, Raman spectra reveal a strong evolution as zirconia content increases (Fig. 4). Indeed, a rising contribution of the band (e) located at about 990 cm^{-1} at the expense of the bands assigned to Q_3(Na,Ca) (i.e. Q_3 units associated with Na^+ and Ca^{2+} ions) and Q_4 units is observed (Fig. 3 and 6). Comparison of the Raman spectra of ZrxNd glasses (x > 0) with that of zektzerite $NaLiZrSi_6O_{15}$ (Fig. 4), shows coincidence of this new band at 990 cm^{-1} with a strong peak present on the zektzerite spectrum, located at 984 cm^{-1}. In zektzerite, this peak can be unambiguously assigned to the stretching mode within Q_3(Zr) units as this mineral phase only contains such units (existence of Zr-O-Si bonds locally charge compensated by Na^+ and Li^+ ions) [55]. As a result, it can logically be suggested that the growing band (e) in ZrxNd and ZrxLa glass series corresponds to a stretching mode within Q_3 units associated with ZrO_6 octahedra (Q_3(Zr)). This is consistent with the increasing number of Si-O-Zr linkages as ZrO_2 content grows up as shown above by Zr-EXAFS. In other Zr-rich silicate crystalline phases such as vlasovite ($Na_2ZrSi_4O_{11}$), zirconium is also 6-fold coordinated but in this case, as there is not enough SiO_2 to enable $(ZrO_6)^{2-}$ entities to be connected only to Q_3

units (Si/Zr = 4), Q_2 units are formed that connect to 2 $(ZrO_6)^{2-}$ entities (existence of Q_2(Zr,Zr) units) [63]. In vlasovite the $(ZrO_6)^{2-}$ entities are thus more distorted than in zekzerite and the vibration bands associated with both Q_3(Zr) and Q_2(Zr,Zr) units can be observed on its Raman spectrum at 989 and 954 cm^{-1} respectively [64]. The band at 989 cm^{-1} in vlasovite that can be associated with Q_3(Zr) units is thus very close to that of zektzerite (984 cm^{-1}). It is interesting to note that the presence of a large band at 975 cm^{-1} was also observed in binary SiO_2-ZrO_2 glasses prepared by sol-gel process and was assigned to a vibrational mode involving mainly Si-O-Zr linkages [65].

For comparison with the complex 7-oxides glasses of the ZrxNd and ZrxLa series (Table 1), we studied the effect of the addition of increasing ZrO_2 amounts on the Raman spectra of simple sodium silicate glasses (Zrx series, Table 2). The composition of this glass series derives from that of a ZrO_2-rich alkali-resistant glass by totally removing Al_2O_3 and replacing all CaO by Na_2O. In comparison with the ZrxRE series, the Zrx series does not contain B_2O_3, Al_2O_3, CaO and RE_2O_3. The evolution of the spectra is shown in Fig. 7. When ZrO_2 content increases, the evolution of the band corresponding to the stretching vibration of the Q_n units is similar for ZrxRE (Figs. 3 and 4) and Zrx series: an increasing contribution is detected on the low energy side of the band (900-1050cm^{-1}) at the expenses of the contribution on its high energy side (1050-1200 cm^{-1}). Similarly to ZrxRE glasses, the Q_n band (800-1250cm^{-1}) was simulated with 3 or 4 Gaussian components for all Zrx glasses (Fig. 8). The position and the attribution of the Gaussian components used for the simulations are given in Table 5 and the evolution of their relative intensities is presented in Fig. 9. For the binary glass Zr0 without ZrO_2, no contribution is observed close to 990 cm^{-1} whereas contributions corresponding to Q_4, Q_3(Na) and Q_2(Na) units are detected. As soon as ZrO_2 is added, a new band of growing intensity appears at about 990cm^{-1}, at the same position as the one detected for the ZrxRE

glasses (Fig. 5, Table 4). This band can be unambiguously assigned to the stretching vibration of Q_3(Zr) units which confirms our band attribution for the ZrxRE series. Simultaneously, a shift towards low energy (from 980 to 936 cm^{-1}) along with an increasing intensity of the band assigned to the Q_2 units is observed (Fig. 9) whereas the contribution of the Q_4 and Q_3(Na) bands significantly decreases. All these results concerning the Zrx series can be explained by the progressive incorporation of ZrO_2 in the silicate network (formation of Si-O-Zr bonds) at the expense of Q_4 and Q_3(Na) entities. Zr can be connected to Q_3 units (forming the Q_3(Zr) units at 990 cm^{-1}) and to Q_2 units. In this latter case, we propose that the Q_2 units can be connected to both Zr and Na (Q_2(Zr,Na) units) or to two Zr (Q_2(Zr,Zr) units) as in the vlasovite structure presented above. The presence of Zr in these new Q_2 units would explain the band shift towards low energy values (44 cm^{-1}) when ZrO_2 is introduced in glass composition (x > 0). In all cases (Q_3(Zr), Q_2(Zr,Na), Q_2(Zr,Zr)), Na^+ ions insure the local charge compensation close to Si-O-Zr bonds.

Angeli et al. [46] in their study on the impact of SiO_2 substitution by ZrO_2 on the structure of soda-lime borosilicate glasses also observed an increasing and important contribution on their Raman spectra at wavenumbers slightly lower than 1000 cm^{-1} that was attributed to the formation of Si-O-Zr linkages. McKeown et al. [58] also put in evidence the increasing contribution of a band at 975 cm^{-1} that they attributed to Q_2 units, in their work on the impact of the addition of ZrO_2 with other waste in alkali borosilicate glasses. In their Raman study on the effect of ZrO_2/K_2O substitution in potassium silicate glasses, Ellison et al. [62] also noticed the presence of a new band near 1010 cm^{-1} that they attributed to the formation of Q_3(Zr) species charge compensated by K^+ ions as in the dalyite mineral phase ($K_2ZrSi_6O_{15}$) [66] and not to the formation of Q_2 species because their vibrational frequencies would occur at lower frequencies. These authors

explained the fact that the band associated with these Q_3(Zr) units was very intense, well resolved and remained at the same position with increasing ZrO_2 content in their glasses by the formation of a relatively well defined local arrangement of Zr^{4+} and K^+ ions near Q_3 units with a more or less fixed stoichiometry. In their work, Ellison et al. [62] also explained the progressive shift towards lower frequency of the stretching vibration of the Q_n(M) bands with the increasing valence of the M cation by the increase of the M-O bond strength that would then weaken the Si-O bond in M-O-Si linkages (M would shift the electron density out of the Si-O bond). In addition to the effect of the mass (Zr being heavier than Na), this would explain why the frequency of the Q_3(Zr) units occurs at a lower value than that of the Q_3(Na,Ca) (ZrxRE series) and Q_3(Na) (Zrx series) bands (Figs. 5 and 8).

According to all previous results, the modifications observed on the Raman spectra of the ZrxRE glass series (Fig. 3 and Fig. 6) can be explained both:

- By the diversion of a fraction of Na_2O (and to a less extent CaO), to react with ZrO_2 and form the $(ZrO_6)^{2-}$ coordination sphere, instead of depolymerizing the network by forming Q_3(Na,Ca) units. This structural effect of ZrO_2 on glass structure is probably mainly responsible of the increase of T_g (Fig. 1c) because Zr-O-Si bonds are stronger than (Na,Ca)-O-Si ones.

- By the introduction in the melt and the incorporation in the silicate network of O^{2-} anions at the same time as Zr^{4+} ions ($2O^{2-}$ anions are brought by each Zr^{4+} ion according to the ZrO_2 formula) that induces a decrease of the amount of Q_4 units (decrease of Si-O-Si linkages) and an increase of Q_3(Zr) (increase of Zr-O-Si linkages). As Zr-O-Si bonds are strong, the impact on T_g of the disruption of the Si-O-Si connections is limited and compensated by the decrease of (Na,Ca)-O-Si(Q_3) connections.

For Zr0Nd and Zr0La glasses without ZrO_2 it was necessary to add a small contribution near 1000 cm^{-1} to simulate the spectra in the 800-1250 cm^{-1} range (Fig. 5a and Table 4). Nevertheless, the contribution of this band becomes insignificant when ZrO_2 is introduced in the glass composition (Fig. 6). By considering both the network modifying role of RE_2O_3 in silicate glasses [17] and several studies reporting the impact of the addition of RE_2O_3 on the Raman spectra of silicate glasses [61,67], it is reasonable to assume that this small contribution is due to the vibration of RE-O-Si(Q_3) units (that can also be referred to as Q_3(RE) units as in Table 4). It is interesting to note that, although the molar amount of RE_2O_3 is similar to the amount of ZrO_2 in the ZrxRE series, the intensity of the Q_3(RE) band is very low compared to the intensity of the Q_3(Zr) band. One possible origin of this effect may lie in the high symmetry of the $(ZrO_6)^{2-}$ octahedron [41], inducing a well-defined structure for the Q_3(Zr) units. Their Raman contributions may add up to form an intense, quite narrow band. Such well-defined structural arrangements may not be found around RE^{3+} centers, because they have a lower field-strength, and because their coordination sphere is surrounded by a larger number of alkali or alkaline earth ions as charge compensators.

4.2.2.2. Aluminum environment

^{27}Al MAS NMR spectra and simulations of ZrxLa glasses are presented in Fig. 10. No spectra evolution is noticeable with increasing ZrO_2 concentration. This clearly demonstrates that the aluminum environment is not significantly affected by increasing ZrO_2 content. The Al environment, characterized by the NMR parameters δ_{iso} = 61.3 - 61.8 ppm and C_Q = 4.5 - 4.7 MHz deduced by simulation (Table 6), is consistent with aluminum occurring mainly as $(AlO_4)^-$ units which is accordance with other WAXS and Molecular Dynamics (MD) studies on aluminoborosilicate glasses [68]. Generally, it is

always observed that in peralkaline aluminoborosilicate glass compositions (i.e. in glasses for which the ratio alkali/Al >1) a great majority of aluminum always occurs in 4-fold coordination and the $(AlO_4)^-$ units are always preferentially charge compensated by alkali ions at the expense of $(BO_4)^-$ units [32,33,68]. This last tendency may be probably explained by the fact that boron can be easily incorporated in the silicate network either as trigonal or tetrahedral species which is not the case for aluminum.

Comparison of the ^{27}Al parameters of ZrxLa glasses with those of reference glasses (Table 7) containing only Na^+ or Ca^{2+} ions as charge compensators (Fig. 11) reveals the strong impact of the nature of the $(AlO_4)^-$ unit charge compensator on NMR parameters. Both quadrupolar coupling constant and chemical shift of ^{27}Al in ZrxLa glasses are similar to the parameters of ^{27}Al in glasses without Ca^{2+} ions. This shows that $(AlO_4)^-$ units always remain totally charge compensated by Na^+ ions in all the glasses of the ZrxLa series. As both Na^+ and Ca^{2+} ions are present in the composition of these glasses (Table 1), this shows that $(AlO_4)^-$ units are preferentially charge compensated by Na^+ rather than by Ca^{2+} ions which can be explained by the preferential reaction in the melt of Al_2O_3 (acid oxide) with the most basic oxide available (Na_2O). This is in accordance with previous results obtained on a similar glass composition where it was shown that $(AlO_4)^-$ units were preferentially charge compensated by Na^+ ions rather than by alkaline earth ions (Mg^{2+}, Ca^{2+}, Sr^{2+}, Ba^{2+}) probably because Na_2O was more basic than the other oxides [33]. Besides, CaO being less basic than Na_2O, prefers to associate to NBOs. This was confirmed by MD simulation results on soda lime silicate [69] and RE-bearing soda lime aluminosilicate [70] glasses that pointed out the fact that Ca^{2+} ions show greater tendency to be surrounded by NBOs than Na^+ ions.

4.2.2.3. Boron environment

Fig. 12 displays the ^{11}B MAS NMR spectra recorded for the ZrxLa samples. Contrary to the results obtained by ^{27}Al MAS NMR (Fig. 10), a strong evolution is observed here which indicates important rearrangement of boron surroundings with increasing ZrO_2 amount. ^{11}B MAS NMR spectra have been simulated considering two contributions for the BO_3 band and a single contribution for the band associated with $(BO_4)^-$ units [20,71]. The proportion N4 of $(BO_4)^-$ units, indicated in Table 8 and reported in Fig. 13 as a function of ZrO_2 content (analyzed content, Table 1), decreases almost linearly with the ZrO_2 concentration. This demonstrates the existence of a competition between $(BO_4)^-$ and $(ZrO_6)^{2-}$ entities for association with charge compensators, which was also reported in [3,46]. At this stage, it should be pointed out that in ZrxLa glasses, preferential charge compensation by sodium rather than by calcium ions occurs for $(BO_4)^-$ entities. Greater affinity of $(BO_4)^-$ entities towards Na^+ ions was shown in [32] and was confirmed in other studies [3,46]. The competition between ZrO_2 and B_2O_3 in favor of ZrO_2 for their association with modifier oxides such as Na_2O and leading to their incorporation in the silicate network as $(ZrO_6)^{2-}$ and $(BO_4)^-$ entities respectively can be explained by the fact that Zr is efficiently solubilized in the glass silicate network only in 6-fold coordination, whereas B easily enters the silicate network as BO_3 units [72].

By considering the composition of Zr0La glass without ZrO_2 (Table 1) and the value of N4 for this glass (46.6%), the hypothetic evolution of N4 with ZrO_2 content in ZrxLa glasses can be estimated if we assume that ZrO_2 "pick up" Na_2O to B_2O_3. This evolution is shown in Fig. 13 (curve (b)) at the same time as the experimental evolution of N4 (curve (a)). It appears that above approximately 3.6 mol% ZrO_2 added to Zr0La glass, all the charge compensator of $(BO_4)^-$ entities would be consumed by the $(ZrO_6)^{2-}$ entities (Fig. 13). The strong divergence between curves (a) and (b) demonstrates that when $x > 0$, Na_2O both contribute to form $(ZrO_6)^{2-}$ and $(BO_4)^-$ units reflecting an

equilibrium between these species. In other terms, the Na_2O amount necessary to form the $(ZrO_6)^{2-}$ entities is in part taken to the amount that would have reacted with B_2O_3, and in part taken to the amount that would have depolymerized the silicate network.

4.2.2.4. Sodium environment

^{23}Na MAS NMR is a useful technique to follow the evolution of the distribution of the Na^+ ions in glass structure [32,73] either in the NBOs-rich regions where they act as modifiers or in the BOs (bridging oxygen atoms)-rich regions where they act as charge compensators near $(BO_4)^-$ or $(AlO_4)^-$ units for instance. Indeed, ^{23}Na NMR parameters δ_{iso} and C_Q are sensitive to sodium local environment in glass. Firstly, $\delta_{iso}(^{23}Na)$ is linearly correlated to the mean Na-O distance in Na-bearing silicate, aluminosilicate and borate crystalline compounds [17,74,75,76] and generally decreases with the mean Na-O distance. More precisely, recent results coupling ^{23}Na NMR, molecular dynamics and density functional calculations have shown that $\delta_{iso}(^{23}Na)$ correlates with the mean Na-O distance in glasses only when the coordination number of sodium is taken into account [73]. Secondly, C_Q is linked to the electric field gradient induced by the negative charge owned by the oxygen atoms present in the neighborhood of the ^{23}Na nuclei (C_Q increases with the negative charge owned by oxygen atoms). According to these considerations, it is expected that when Na^+ ions act as modifiers near NBOs, their δ_{iso} and C_Q parameters are higher than when they act as charge compensators near $(BO_4)^-$ or $(AlO_4)^-$ units for which the negative charge is delocalized on four oxygen atoms. This is verified in Fig. 14 where is presented the evolution of the δ_{iso} and C_Q parameters for a set of simple Na_2O-bearing silicate, borate, borosilicate and aluminosilicate reference glasses in which the environments of Na^+ ions are significantly different (Table 9, blue circles in Fig. 14). The

^{23}Na MAS NMR spectra and simulations of these reference glasses are presented in Fig. 15. Among these reference glasses two kinds of compositions can be distinguished:

- Glasses for which Na^+ ions only play the role of charge compensators near $(AlO_4)^-$ units (this is the case of the SiAlNa glass, for which there is just enough Na_2O to compensate all $(AlO_4)^-$ tetrahedra) or $(BO_4)^-$ units (this is the case of the B0.2Na glass, for which there is no NBO and all Na_2O is used to compensate $(BO_4)^-$ tetrahedra). These glasses correspond to the domain at the bottom left in Fig. 14 (low δ_{iso} and C_Q).

- Glasses for which all or at least a great proportion of Na_2O act as modifier by forming NBOs on SiO_4 (SiNa, SiNaCa, SiNaLa glasses) or BO_3 (B0.7Na glass) units. In silicate glasses structure, Na^+ ions are surrounded by both NBOs (from Q_n units with $n < 4$) and BOs (from Si-O-Si bonds). These reference glasses correspond to the domain at the top right in Fig. 14 (high δ_{iso} and C_Q).

In Fig. 14 is also reported the evolution of the ^{23}Na NMR parameters of Zrx glasses (Table 9, green triangles in Fig. 14). The corresponding MAS NMR spectra are presented in Fig. 16. It appears that the introduction of ZrO_2 (5-10 mol%) in the Zr0 glass (a binary sodium silicate glass in which all Na^+ ions play a modifier role as in the SiNa reference glass, Fig 14) induces a significant decrease of the values of δ_{iso} and C_Q of ^{23}Na. This evolution can be explained by an increasing amount of Na^+ ions acting as charge compensators near $(ZrO_6)^{2-}$ units. Indeed, an increasing amount of Na_2O (close to 42 and 84% respectively in the Zr5 and Zr10 glasses, Table 9) is expected to be mobilized as charge compensator in these ZrO_2-bearing glasses which induces an increase of the mean Na-O distance (decrease of δ_{iso}) whereas the mean electric field gradient at ^{23}Na nuclei decreases (decrease of C_Q). The increase of the mean Na-O distance is expected to increase according to bond valence - bond length considerations [37,43] Indeed, the bond

valence between a Na^+ ion and a NBO is higher than the bond valence between a Na^+ ion and an oxygen atom in a Zr-O-Si bond.

The experimental and simulated ^{23}Na MAS NMR spectra of the glasses of the ZrxLa series are shown in Fig. 17. The parameters extracted from the simulation of these spectra are given in Table 9 and their evolution is presented in Fig. 14 (red circles). It appears that the δ_{iso} and C_Q parameters of all these glasses are located on the bottom left of the figure. This can be explained by the fact that even for the glass without ZrO_2 (Zr0La glass) a high proportion of Na^+ ions is already used to compensate the $(BO_4)^-$ and $(AlO_4)^-$ units (48 mol% if we assumed that these units are only compensated by Na^+ ions, Table 9). When adding ZrO_2, as for the Zrx series the total amount of Na_2O acting as charge compensator increases due to the formation of $(ZrO_6)^{2-}$ units (until 84% if we assumed that these units are only compensated by Na^+ ions, Table 9) in spite of the decrease of the amount of $(BO_4)^-$ units (Table 8). This explains the shift of δ_{iso} towards lower values that is observed at the same time as the decrease of C_Q for the ZrxLa glasses when adding increasing ZrO_2 amount (Fig. 14).

The effect of ZrO_2 on the distribution of charge compensators and modifiers is summarized by the structural scheme shown in Fig. 18. It is interesting to note that according to our results, an increasing proportion of Na^+ ions previously acting as modifiers in the NBOs-rich regions of the glass structure (DR in Fig. 18) for the lowest ZrO_2 contents is progressively displaced towards the polymerized regions (PR in Fig. 18) where they act as charge compensators. This evolution is expected to affect the environment - and thus the solubilization - of RE^{3+} ions in the glass, these ions being preferentially located in the NBOs-rich regions of the glass structure where it is easier to satisfy their environment. This point is developed in another paper [36].

4.2.2.5. Silicon environment

The ^{29}Si MAS NMR spectra of the glasses of the ZrxLa series are shown in Fig. 19. The spectra are very similar for all glasses, they are wide and not resolved (the contribution of different kinds of Q_n units cannot be detected on the spectra) which can be explained by the existence of numerous kinds of different environments for the Q_n units in the aluminoborosilicate glassy network that induces a widening of the spectra (existence of Si-O-Si, Si-O-Al, Si-O-B, Si-O-Zr, Si-O-Na, Si-O-Ca and Si-O-La bonds). Indeed, the chemical shift of Q_n units depends both on their number (4-n) of NBOs and on the nature of their second neighbors [77]. Only a very slight variation of the maximum of the spectra towards high chemical shifts (about 1-2 ppm) is observed when the ZrO_2 content increases that could be due to the presence of Zr as second neighbor of Q_n units in accordance with the results of the NMR study of Lapina et al. [78] on silica fiberglass modified by ZrO_2. A slight shift of the ^{29}Si NMR peak in the same direction was also observed by Angeli et al. [46] when they substituted SiO_2 by ZrO_2 in a soda-lime borosilicate glass. Nevertheless, it is very difficult to conclude with certainty because when the ZrO_2 content increases, the variations of local environment in the surrounding of SiO_4 units are very complex according to the previous sections and the relative proportions of the different kinds of Si-O-M bonds (M = Si, Al, B, Zr, Na, Ca, La) change: evolution of the coordination of boron atoms (BO_4, BO_3) connected to Si, redistribution of Na^+ and Ca^{2+} ions in the neighbourhood of Q_n units with $n < 4$ due to the preferential charge compensation of $(ZrO_6)^{2-}$ entities by Na^+ ions, increasing amount of Si-O-Zr bonds. All these local structural changes may affect the chemical shift of ^{29}Si in opposite directions finally leading to compensating effects [32,46,77,79] which probably explains the very slight evolution of ^{29}Si NMR spectra with ZrO_2 content (Fig. 19). However, it is interesting to compare the evolution of the ^{29}Si MAS NMR spectra of the

ZrxLa glasses with that of the glasses of the Zrx series (without B, Al, Ca and La) shown in Fig. 20. For the Zrx series, a significant evolution of the spectra is put in evidence with the introduction of increasing ZrO_2 content in the binary sodium silicate Zr0 glass. Whereas without ZrO_2 the contributions of Q_4 and Q_3(Na) units are clearly resolved (Zr0 glass) [80], the spectra of Zrx glasses (x = 5, 10) shift towards higher chemical shifts and become narrower when ZrO_2 is added, showing a significant decrease of the contribution of Q_4 units and the occurrence of an increasing contribution centred at about -98 ppm probably associated with the formation of Q_3(Zr) units charge compensated by Na^+ ions at the expense of Q_4 and Q_3(Na) units in accordance with the Raman results presented above for this series. A similar structural evolution probably occurs for the glasses of the ZrxLa series which would explain the slight shift of the spectra with ZrO_2 content (Fig. 19) but is not as obvious as that put in evidence for the Zrx glasses because of the higher chemical complexity of ZrxLa glasses.

5. Conclusions

Strong impact of ZrO_2 addition on the structural features of a simplified RE-bearing aluminoborosilicate nuclear glass (RE = Nd, La) was put in evidence, demonstrating the important role of zirconium in this glass system. From a multi-spectroscopic approach (Zr-EXAFS, multinuclear (^{11}B, ^{23}Na, ^{27}Al, ^{29}Si) MAS NMR, Raman) specific focuses on the elements - formers and modifiers - constituting the glass structure have been performed and enabled to draw the structural changes occurring when ZrO_2 is added to the glass in increasing amount. Zirconium appears intimately incorporated in the glass matrix, forming regular $(ZrO_6)^{2-}$ octahedra connected to the silicate network through Zr-O-Si bonds and preferentially charge compensated by Na^+ rather than by Ca^{2+} ions. While aluminium remains unaffected as tetrahedral $(AlO_4)^-$ units charge compensated by Na^+

ions, it was demonstrated that increasing Zr content induces significant changes in the borosilicate network structure: formation of Zr-O-Si(Q_3) units at the expense of Q_4 and Q_3(Na) units and decrease of the proportion of $(BO_4)^-$ units due to the mobilization of Na^+ ions for $(ZrO_6)^{2-}$ charge compensation. The fact that the amount of Na^+ ions released by partial transformation of $(BO_4)^-$ into BO_3 units was not sufficient to charge compensate all $(ZrO_6)^{2-}$ units justifies partial transformation of Q_3(Na) into Q_3(Zr) units reducing at the same time the amount of NBOs in glass structure.

According to all the results presented in this paper, it may be expected that the preferential charge compensation mechanism of zirconium induces at the same time a decrease of the amount of NBOs and an increase of the relative proportion of Ca^{2+} ions in the depolymerized regions of the structure where are located RE^{3+} ions (Fig. 18). The environment of these ions is thus probably significantly modified and their stability affected by ZrO_2 addition. This is confirmed in another paper [36] by following directly the evolution of the local environment of RE^{3+} ions and the glass crystallization tendency with ZrO_2 content.

Acknowledgments

The authors thank the CEA and the AREVA Chaire with Chimie-ParisTech and ENSTA-ParisTech for their contribution to the financial support of this study. We would also like to acknowledge the members of the ANKA synchrotron (INE beamline, Karlsruhe, Germany) for their help and availability during the Zr K-edge EXAFS experiments. D. R. Neuville and D. de Ligny are gratefully acknowledged for giving us the possibility to use the Raman spectrometers of the Institut de Physique du Globe (Paris, France) and of the Institut Lumière Matière (Lyon, France).

Glass (mol%)	SiO_2	B_2O_3	Al_2O_3	Na_2O	CaO	ZrO_2	RE_2O_3	T_g(°C)
Zr0RE[a]	63.00	9.12	3.11	14.69	6.45	0	3.63	
Zr0Nd[b]	64.15	8.13	3.27	14.06	6.74	0	3.66	602 (Nd)
Zr0La[b]	62.56	7.85	3.50	14.91	7.07	0	4.10	593 (La)
Zr1RE[a]	61.81	8.94	3.05	14.41	6.33	1.90	3.56	
Zr1Nd[b]	60.39	8.56	3.31	14.93	7.04	2.04	3.73	611 (Nd)
Zr1La[b]	60.91	8.63	3.14	14.50	6.88	1.93	4.00	600 (La)
Zr2RE[a]	60.61	8.77	2.99	14.14	6.20	3.79	3.49	
Zr2Nd[b]	60.41	8.51	3.20	13.63	6.45	4.19	3.62	632 (Nd)
Zr2La[b]	60.45	7.48	3.27	14.00	6.78	4.17	3.83	615 (La)
Zr3RE[a]	59.42	8.60	2.94	13.86	6.08	5.69	3.42	
Zr3Nd[b]	58.41	8.51	3.15	13.65	6.48	6.24	3.56	642 (Nd)
Zr3La[b]	57.45	7.34	3.40	14.34	6.96	6.57	3.91	640 (La)

Table 1. ([a]) Theoretical composition of ZrxRE glasses (RE = Nd or La). ([b]) Analyzed compositions of all ZrxNd and ZrxLa glasses by ICP AES are also given for comparison. Increasing amount of ZrO_2 was added to Zr0RE glass at the expense of all other oxides. For all glasses of the ZrxLa series, 0.15 mol% Nd_2O_3 was introduced to reduce the relaxation time during NMR study (the RE_2O_3 concentration given in Table 1 for RE = La corresponds to La_2O_3 + Nd_2O_3). The glass transformation temperature T_g (uncertainty +/- 3°C) determined by DTA is given in the last column.

Glass (mol%)	SiO_2	Na_2O	ZrO_2	Na_2O/SiO_2	Na_2O/ZrO_2
Zr0[a]	77.77	22.22	0	0.285	-
Zr0[b]	85.22	14.28	0	0.167	-
Zr5[a]	73.68	21.05	5.26	0.285	4.00
Zr5[b]	80.68	13.57	5.74	0.168	2.36
Zr10[a]	70.00	20.00	10.00	0.285	2.00
Zr10[b]	76.27	12.91	10.82	0.169	1.19

Table 2. ([a]) Theoretical composition of sodium silicate glasses (Zrx series) with increasing ZrO_2 content. ([b]) Analyzed compositions of Zrx glasses by ICP AES are given for comparison. For Zr5 and Zr10 glasses, increasing amount of ZrO_2 was added to the Zr0 glass at the expense of all other oxides. Due to strong Na_2O evaporation during melting at 1560°C, nominal and true Na_2O/ZrO_2 ratios are significantly different. The theoretical and analyzed Na_2O/SiO_2 and Na_2O/ZrO_2 ratios are also given.

Glass	Zr-O(Å)	CN	σ^2(Å^2)
Zr1Nd	2.09(1)	6.0(0.9)	0.0050(5)
Zr3Nd	2.09(1)	6.0(0.9)	0.0051(5)
Glass	**Zr-Si(Å)**	**CN**	**σ^2(Å^2)**
Zr1Nd	3.37(2)	1.4(1.0)	0.002(2)
Zr3Nd	3.36(2)	1.7(1.2)	0.004(4)
	Zr-O(Å)	**CN**	**σ^2(Å^2)**
Zektzerite	2.08	5.9	0.0036
Glass G1	2.15	6.5	0.007
Glass G2	2.14	5.5	0.006

Table 3. Zr K-edge EXAFS best-fit parameters of the Zr-O (1st neighbors) and Zr-Si shells (2nd neighbors) in Zr1Nd and Zr3Nd glasses (mean Zr-O distance, coordination number CN, Debye-Waller factor σ^2). EXAFS parameters taken from literature for synthetic crystalline zektzerite ($LiNaZrSi_6O_{15}$) [38] and (Zr,Ca)-bearing silicate glasses (G1 [81], G2 [82]) are also given (glass G1 (mol%): 48.8 SiO_2 - 8.5 Al_2O_3 - 25.3 CaO - 11.3 TiO_2 - 5.0 ZrO_2 - 1.1 Na_2O; glass G2 (mol%): 55.70 SiO_2 - 39.78 CaO - 4.52 ZrO_2). Mean square deviations applying on last digits are indicated in parenthesis.

Glass	Zr0Nd	Zr1Nd	Zr2Nd	Zr3Nd	Zr0La	Zr1La	Zr2La	Zr3La
Q_4	1150	1150	1150	1150	1150	1150	1150	1150
Q_3(Na,Ca)	1066	1065	1064	1064	1063	1062	1063	1061
Q_3(Zr,Nd,La)	1003	990	990	990	998	990	990	990
Q_2	957	934	935	937	953	936	937	938

Table 4. Position (in cm^{-1}) of the Gaussian components used to simulate the Raman spectra (800-1250 cm^{-1}) of the glasses of ZrxLa and ZrxNd series (Fig. 5). For Zr0La and Zr0Nd glasses (without RE), the Q_3 component around 1000 cm^{-1} corresponds to the stretching vibration of respectively Q_3(La) and Q_3(Nd) entities whereas for all glasses containing ZrO_2 this component mainly corresponds to the stretching vibration of Q_3(Zr) entities. For all simulations, the position of the Q_4 band was fixed at 1150cm^{-1} and for all glasses with ZrO_2, the position of the Q_3(Zr) band was fixed at 990 cm^{-1}.

Glass	Zr0	Zr5	Zr10
Q_4	1170	1170	-
Q_3(Na)	1095	1090	1076
Q_3(Zr)	-	992	988
Q_2	980	940	936

Table 5. Position (in cm^{-1}) of the Gaussian components used to simulate the Raman spectra (800-1250 cm^{-1}) of the glasses of the Zrx series (Fig. 8). For Zr10 glass, it was not possible to separate the contribution of a band associated with the vibration of Q_4 units, thus the Q_3(Na) band probably includes the Q_4 contribution.

Glass	δ_{iso} (ppm) (±0.1)	gb	C_Q (MHz) (±0.1)	η
Zr0La	61.3	4.4	4.5	0.6
Zr1La	61.6	4.4	4.5	0.6
Zr2La	61.6	4.4	4.6	0.6
Zr3La	61.8	4.3	4.7	0.6

Table 6. NMR parameters deduced from the simulation of ^{27}Al MAS NMR spectra of glasses of the ZrxLa series (Fig. 10). δ_{iso} is the mean isotropic chemical shift. gb represents the dispersion of chemical shift (standard deviation value of the Gaussian distribution used in the simulation). C_Q is the mean quadrupolar coupling constant. The mean asymmetry parameter η is constant and fixed to 0.6 in these simulations.

Glass	SiO_2	Al_2O_3	B_2O_3	Na_2O	CaO	ZrO_2	La_2O_3
A	58.47	8.89	6.00	-	26.62	-	-
B	61.81	3.05	8.94	-	20.74	1.90	3.56
C	76.92	11.54	-	11.54	-	-	-
D	61.81	3.05	8.94	20.74	-	1.90	3.56

Table 7. Composition (mol%) of the reference glasses A, B, C and D used for the ^{27}Al MAS NMR study of the glasses of the ZrxLa series (Fig. 11). Glass A only contains Ca^{2+} ions to charge compensate $(AlO_4)^-$ units and has a composition close to that of the industrial E-glass used as fibers to reinforce plastics. Glasses B and D are glasses of similar compositions but that contain either only Ca^{2+} or Na^+ ions to charge compensate $(AlO_4)^-$ units and that were studied in [32,38]. Glass C only contains Na^+ ions to charge compensate $(AlO_4)^-$ units.

	BO_4				BO_3 (1)				BO_3 (2)			
Glass	**%**	**δ_{iso} (ppm)**	**C_Q (MHz)**	**η**	**%**	**δ_{iso} (ppm)**	**C_Q (MHz)**	**η**	**%**	**δ_{iso} (ppm)**	**C_Q (MHz)**	**η**
Zr0La	46.6	-0.61	0.35	0.6	34.7	17.9	2.5	0.34	18.7	14.0	2.8	0.37
Zr1La	41.6	-0.53	0.35	0.6	38.6	17.8	2.5	0.34	19.8	14.0	2.8	0.45
Zr2La	37.0	-0.55	0.35	0.6	49.2	17.9	2.6	0.40	13.8	14.0	2.8	0.38
Zr3La	29.2	-0.52	0.35	0.6	54.1	17.9	2.6	0.40	16.7	14.0	2.8	0.43

Table 8. NMR parameters and ratios (in %) of BO_4 and BO_3 species deduced from the simulation of ^{11}B MAS NMR spectra of glasses of the ZrxLa series (Fig. 12). The two BO_3 contributions required to get correct fitting of the spectra are consistent with BO_3 ring ($BO_3(1)$) and BO_3 non ring ($BO_3(2)$) found in literature [46]. Contrarily to what is sometimes done in literature [46], the BO_4 contribution was fitted by considering only one contribution. δ_{iso} is the mean isotropic chemical shift. C_Q is the mean quadrupolar coupling constant. η is the asymmetry parameter.

Glass	δ_{iso} (ppm)	gb	C_Q (MHz)	η	$\%Na_2O_{comp}$
Zr0La	-7.2	8.3	2.4	0.6	48
Zr1La	-7.3	8.2	2.3	0.6	59.7
Zr2La	-8.4	8.1	2.2	0.6	72.9
Zr3La	-9.0	8.0	2.2	0.6	84.5
Zr0	3.93	9.16	3.53	0.6	0
Zr5	-0.95	9.69	3.18	0.6	42.3
Zr10	-4.33	9.34	2.80	0.6	83.8

Table 9. NMR parameters deduced from the simulation of ^{23}Na MAS NMR spectra of glasses of the ZrxLa and Zrx series (Figs. 15 and 16). δ_{iso} is the mean isotropic chemical shift. gb represents the distribution of chemical shift (standard deviation value of the Gaussian distribution used in the simulation). C_Q is the mean quadrupolar coupling constant. The mean asymmetry parameter η is constant and fixed to 0.6 in these simulations. The last column corresponds to the amount of Na_2O (in mol%) acting as charge compensator of $(BO_4)^-$, $(AlO_4)^-$ and $(ZrO_6)^{2-}$ units in the ZrxLa series taking into account ^{11}B and ^{27}Al NMR results (showing that all is Al in four-fold coordination and giving $\%BO_4$) assuming that all these units are only compensated by Na^+ ions. For the Zrx series, two Na^+ ions were supposed to compensate one $(ZrO_6)^{2-}$ unit.

Glass	SiO_2	Al_2O_3	B_2O_3	Na_2O	CaO	La_2O_3	Nd_2O_3	δ_{iso} (ppm)	gb	C_Q (MHz)
SiNa	80.93	-	-	19.07	-	-	-	3.22	9.2	3.65
SiNaCa	71.21	-	-	16.78	12.01	-	-	-0.46	9.3	3.06
SiAlNa	76.92	11.54	-	11.54	-	-	-	-14.03	7.7	2.16
SiNaLa	74.38	-	-	21.29	-	4.18	0.15	-0.10	9.0	3.19
B0.2Na	-	-	83.3	16.7	-	-	-	-9.58	7.2	2.35
B0.7Na	-	-	58.8	41.2	-	-	-	2.83	8.4	3.06

Table 10. Composition (mol%) of Na_2O-bearing reference silicate, borate, aluminosilicate and borosilicate glasses prepared by the authors for various studies and used here for comparison of their ^{23}Na NMR parameters with those of the glasses of the ZrxLa series. The experimental and simulated ^{23}Na MAS NMR spectra of some of these glasses are shown in Fig. 15. The δ_{iso}, gb and C_Q parameters of these glasses determined by spectra simulation are reported in the Table. In SiNa, SiNaCa and SiNaLa glasses, Na^+ ions only play the role of modifiers near NBOs either alone or with Ca^{2+} and La^{3+} ions. In SiAlNa and B0.2Na glasses, Na^+ ions only play the role of charge compensators near respectively $(AlO_4)^-$ and $(BO_4)^-$ units. In B0.7Na glass, Na^+ ions play the role of modifiers near $(BO_3)^-$ units and the role of charge compensators near $(BO_4)^-$ units.

Figures captions

Fig. 1. Evolution with ZrO_2 content of the: (a) density (uncertainty < ± 0.004), (b) oxygen molar volume Vm(Ox) and (c) glass transformation temperature T_g for the glasses of the ZrxNd and ZrxLa series.

Fig. 2. Modulus of the Fourier transform of the k^3-weighted Zr K-edge EXAFS function for Zr1Nd and Zr3Nd glasses. The inset (top right) shows the local structure in the surrounding of Zr with preferential charge compensation by Na^+ ions.

Fig. 3. Raman spectra of ZrxNd glasses in the 100-1600 cm^{-1} range. After correction by Long formula and subtraction of a third-order polynomial baseline, the spectra were normalized to total unit area.

Fig. 4. Raman spectra of ZrxNd glasses in the 800-1250 cm^{-1} range: (a) Zr0Nd, (b) Zr1Nd, (c) Zr2Nd, (d) Zr3Nd. The Raman spectrum (e) of natural zektzerite ($LiNaZrSi_6O_{15}$) is shown for comparison [83]. The inset (top left) shows the connection between Q_3 and $(ZrO_6)^{2-}$ units in structure of zekzerite ($LiNaZrSi_6O_{15}$) with local charge compensation insured by Na^+ or Li^+ ions.

Fig. 5. (top) Raman spectrum (a) and Gaussian fitting (b) of the Zr0Nd glass with four Gaussian bands associated with the following SiO_4 units: Q_4 (c), Q_3(Na,Ca) (d), Q_3(Nd) (e), Q_2 (f). (bottom) Raman spectrum (a) and Gaussian fitting (b) of the Zr3Nd glass with four Gaussian bands associated with the following SiO_4 units: Q_4 (c), Q_3(Na,Ca) (d), Q_3(Zr) (e), Q_2 (f). For clarity reason experimental spectra (a) have been slightly shifted towards the top of the figures.

Fig. 6. Relative contribution of the different bands assigned to the SiO_4 units in ZrxNd (a) and ZrxLa (b) glasses versus the ZrO_2 nominal content, according to the fitting of the Raman spectra shown in Fig. 5.

Fig. 7. Raman spectra of glasses of the Zrx series in the 300-1300 cm^{-1} range. The spectra were normalized to their maximum intensity.

Fig. 8. Raman spectra (a) and Gaussian fitting (b) of glasses of the Zrx series with three or four Gaussian bands associated with the following SiO_4 units: Q_4 (c), Q_3(Na) (d), Q_3(Zr) (e), Q_2 (f).

Fig. 9. Relative contribution of the different bands assigned to the SiO_4 units in Zrx glasses according to the fitting of the Raman spectra shown in Fig. 8.

Fig. 10. Experimental (solid lines) and simulated (dashed lines) normalized ^{27}Al MAS NMR spectra of the glasses of the ZrxLa series.

Fig. 11. Evolution with the ZrO_2 content of the mean C_Q and δ_{iso} parameters deduced from the simulation of ^{27}Al MAS NMR spectra of glasses of the ZrxLa series (Fig. 10, Table 6)**.** Glasses A, B, C and D (Table 7) are reference glasses for which aluminum mainly occurred in 4-fold coordination and is mainly or totally charge compensated by Ca^{2+} (glasses A and B) or Na^+ (glasses C and D) ions. The domains surrounded by dotted lines in the figure separate glasses for which $(AlO_4)^-$ units are mainly charge compensated by Ca^{2+} ions or by Na^+ ions. These reference glasses have been used to compare their NMR parameters after spectra simulation with those of the glasses of the ZrxLa series in order to identify the nature and follow the evolution of charge compensation mode of the (AlO_4^-) units in our ZrO_2 bearing glasses.

Fig. 12. Normalized ^{11}B MAS NMR spectra of the glasses of the ZrxLa series.

Fig. 13. (a) Evolution of the relative proportion of BO_4 units versus the amount of ZrO_2 in glasses ZrxLa (a linear fit is also shown) as determined by ^{11}B MAS NMR (Table 8) (b) Expected evolution of the relative proportion of BO_4 units with ZrO_2 content if all $(ZrO_6)^{2-}$ octahedra present in ZrxLa glasses are associated with charge compensators that initially compensate the $(BO_4)^-$ units in the Zr0La glass (i.e. the glass without ZrO_2).

Fig. 14. Evolution of the mean C_Q and δ_{iso} parameters deduced from the simulation of ^{23}Na MAS NMR spectra of the ZrxLa glass series (Fig. 17) as well as a set of Na_2O-bearing reference and Zrx glasses (Figs. 15 and 16). This figure points out two domains grouping reference glasses in which Na^+ ions are mainly present in the vicinity of NBOs (black dotted line) and glasses in which Na^+ ions mainly act as charge compensator near $(AlO_4)^-$ or $(BO_4)^-$ units (green dotted line).

Fig. 15. Experimental (solid lines) and simulated (dashed lines) ^{23}Na MAS NMR spectra of Na_2O-bearing silicate, borate, aluminosilicate and borosilicate reference glasses (Table 10).

Fig. 16. Experimental ^{23}Na MAS NMR spectra of the glasses of the Zrx series (Table 2).

Fig. 17. Experimental (solid lines) and simulated (dashed lines) normalized ^{23}Na MAS NMR spectra of the glasses of the ZrxLa series.

Fig. 18. Schematic bidimensional representation of the structure of a peralkaline RE-bearing aluminoborosilicate glass containing sodium, calcium and RE = Nd. This figure shows: SiO_4 units without (Q_4) and with NBOs (Q_n $n < 4$) associated with Na^+ and Ca^{2+} ions; $(AlO_4)^-$, $(BO_4)^-$ and $(ZrO_6)^{2-}$ units mainly charge compensated by Na^+ ions and connected to the silicate network; BO_3 triangles; Nd^{3+} ions connected to the silicate network with their nearest NBOs neighbors associated with Na^+ or Ca^{2+} to locally compensate the negative charge excess of the Nd-O-Si bonds. Examples of bridging oxygen atoms (BOs) and non-bridging oxygen atoms (NBOs) are shown. Depolymerized regions (i.e. NBOs-rich regions) are indicated by DR in the figure and are separated by polymerized regions (i.e. BO-rich regions) that are indicated by PR in the figure. The dotted lines separate DR and PR regions in the figure. The possible presence of BO_4 tetrahedral units as next-nearest neighbors of Nd^{3+} ions is also proposed in the figure. The structural scheme shown in this figure (RE-bearing aluminoborosilicate glasses not

homogeneous at the nanometric scale) is inspired by the model proposed by Greaves for silicate glasses [84,85]. The green arrows indicate the effect of the formation of $(ZrO_6)^{2-}$ units on the distribution of Na^+ ions in the surrounding of Nd^{3+} ions (decrease of the total amount of charge compensators available and increase of the Ca/Na ratio) and on the partial conversion of $(BO_4)^-$ into BO_3 units.

Fig. 19. Normalized ^{29}Si MAS NMR spectra of the glasses of the ZrxLa series. Q_n range of chemical shift in silicate glasses for Q_n units connected to n silicon atoms and (4-n) NBOs are shown [77].

Fig. 20. Normalized ^{29}Si MAS NMR spectra of the glasses of the Zrx series.

Figure 1

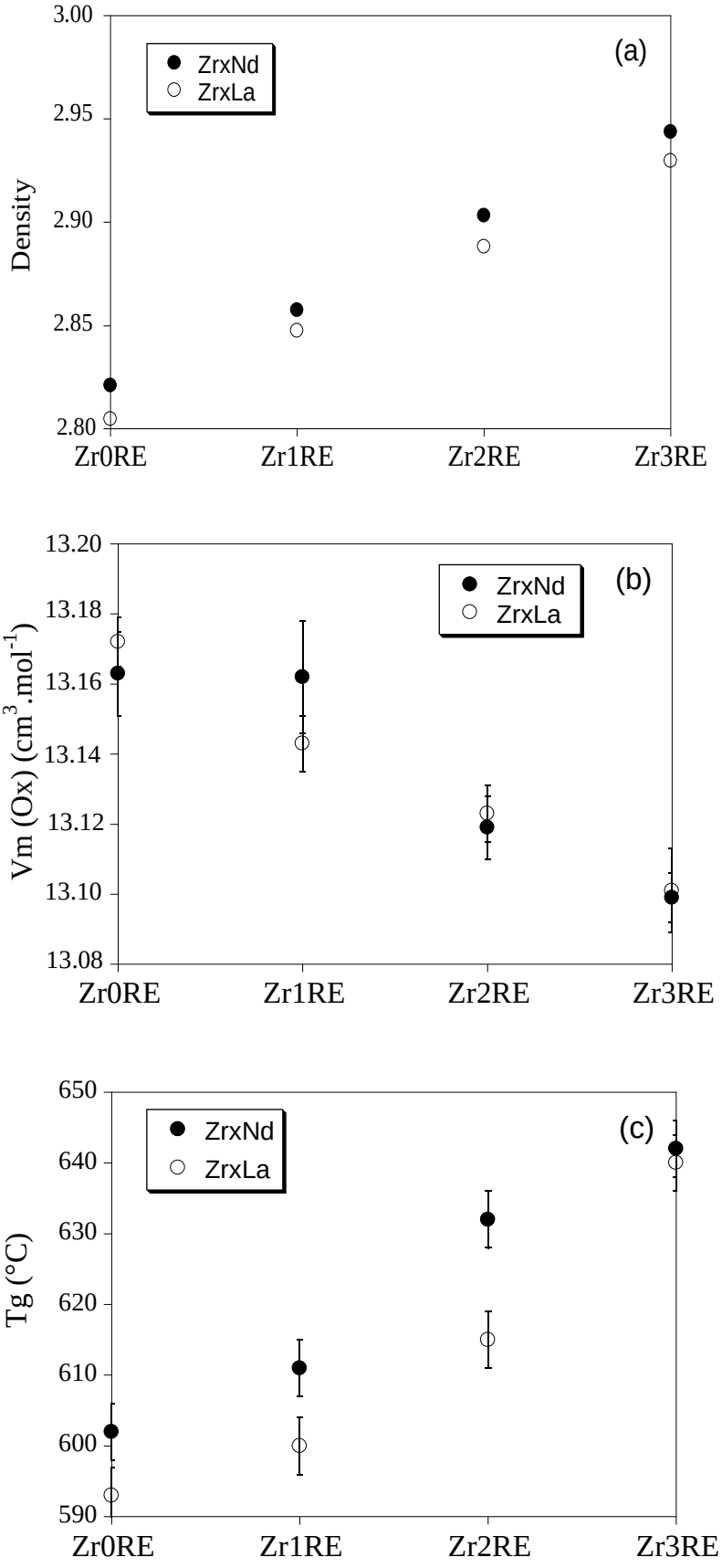
(a)
ZrxNd
ZrxLa
Density
3.00
2.95
2.90
2.85
2.80
Zr0RE
Zr1RE
Zr2RE
Zr3RE
(b)
ZrxNd
ZrxLa
Vm (Ox) (cm3.mol-1)
13.20
13.18
13.16
13.14
13.12
13.10
13.08
Zr0RE
Zr1RE
Zr2RE
Zr3RE
(c)
ZrxNd
ZrxLa
Tg (°C)
650
640
630
620
610
600
590
Zr0RE
Zr1RE
Zr2RE
Zr3RE

Figure 2

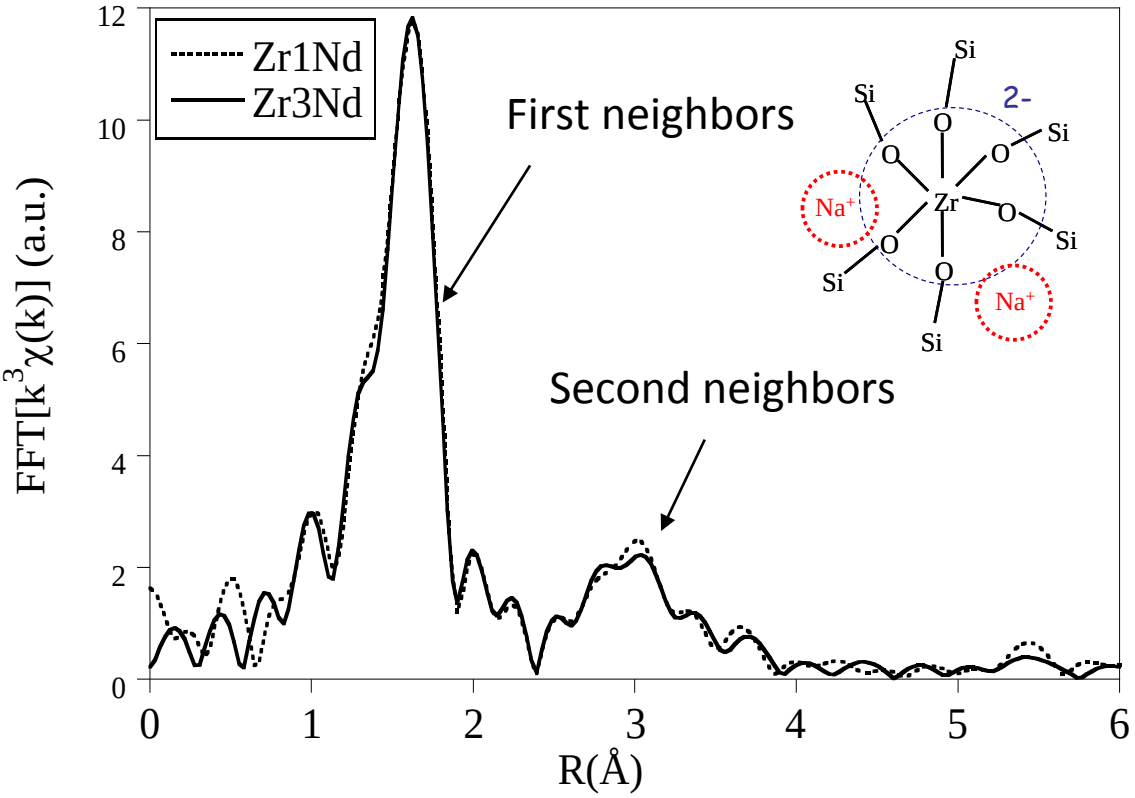
Zr1Nd
Zr3Nd
First neighbors
Second neighbors
FFT[k3χ(k)] (a.u.)
R(Å)
0
2
4
6
8
10
12
0
1
2
3
4
5
6
Si
O
Zr
Na+
2-

Figure 3

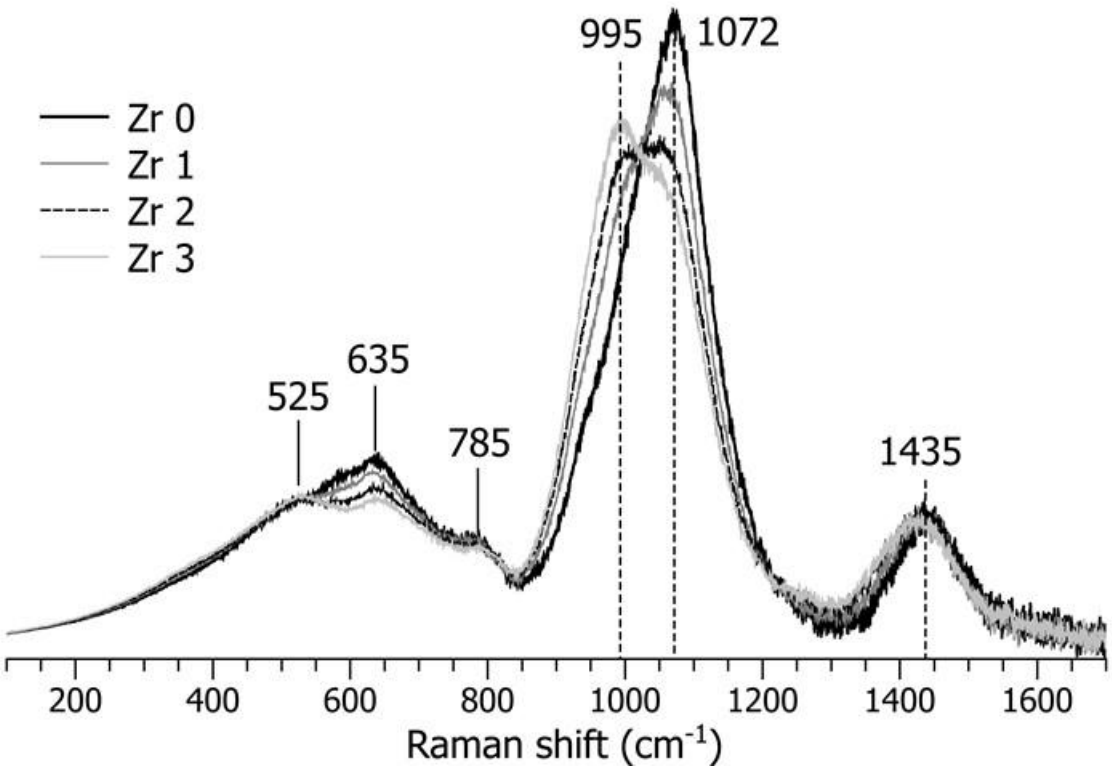
995
1072
Zr 0
Zr 1
Zr 2
Zr 3
635
525
785
1435
200
400
600
800
1000
1200
1400
1600
Raman shift (cm-1)

Figure 4

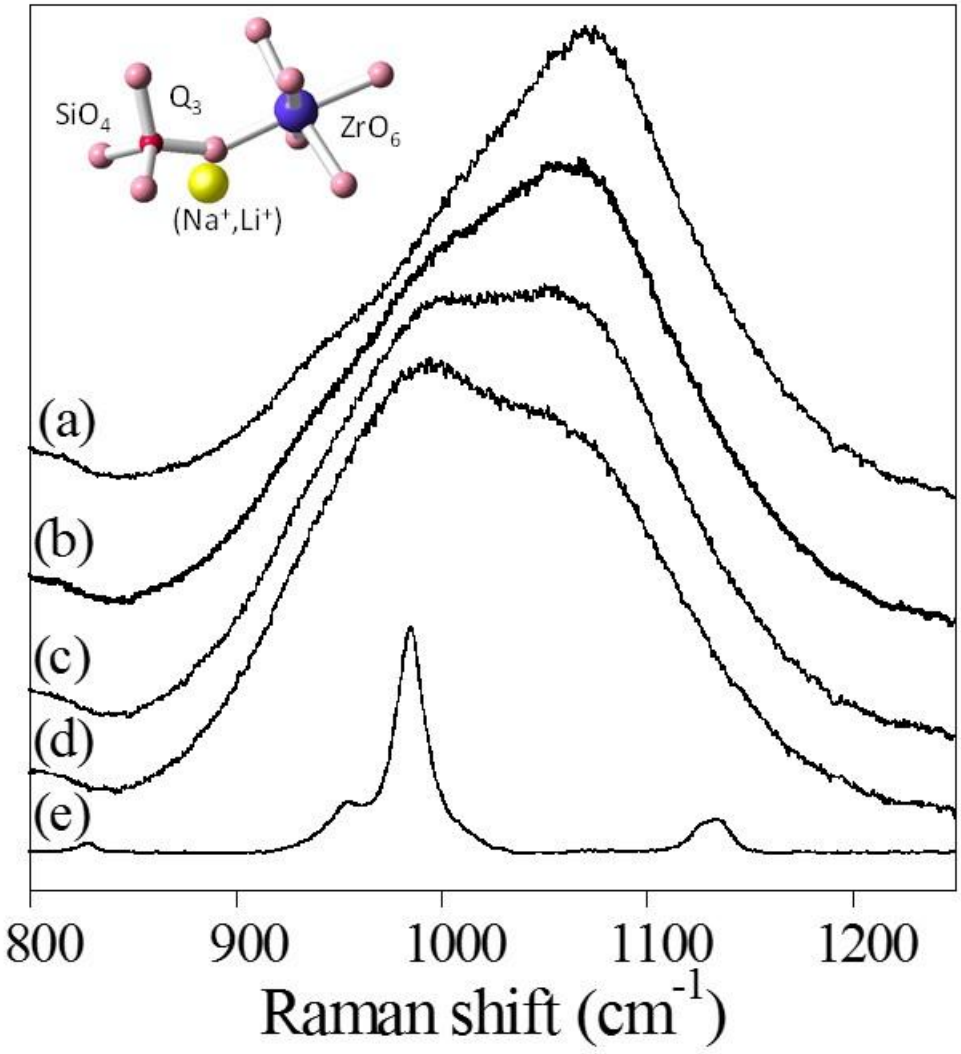
SiO4
Q3
ZrO6
(Na+,Li+)
(a)
(b)
(c)
(d)
(e)
800
900
1000
1100
1200
Raman shift (cm-1)

Figure 5

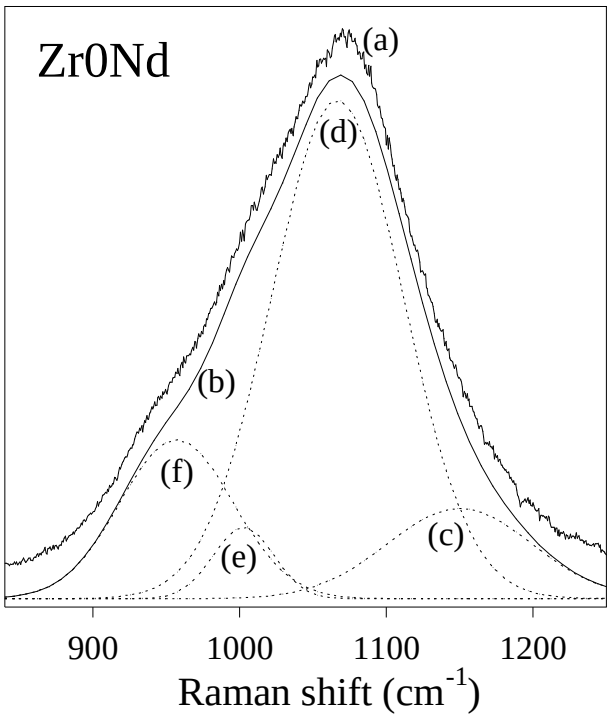
Zr0Nd
(a)
(d)
(b)
(f)
(e)
(c)
900
1000
1100
1200
Raman shift (cm-1)

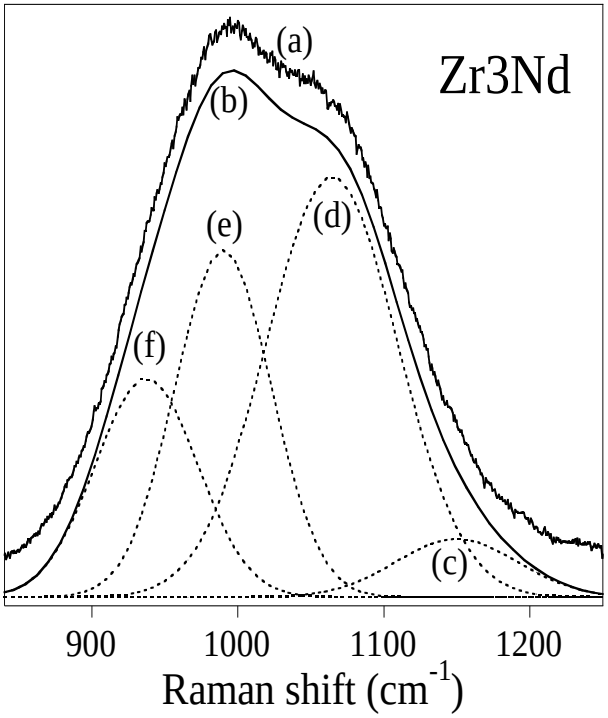
Zr3Nd
(a)
(b)
(e)
(d)
(f)
(c)
900
1000
1100
1200
Raman shift (cm-1)

Figure 6

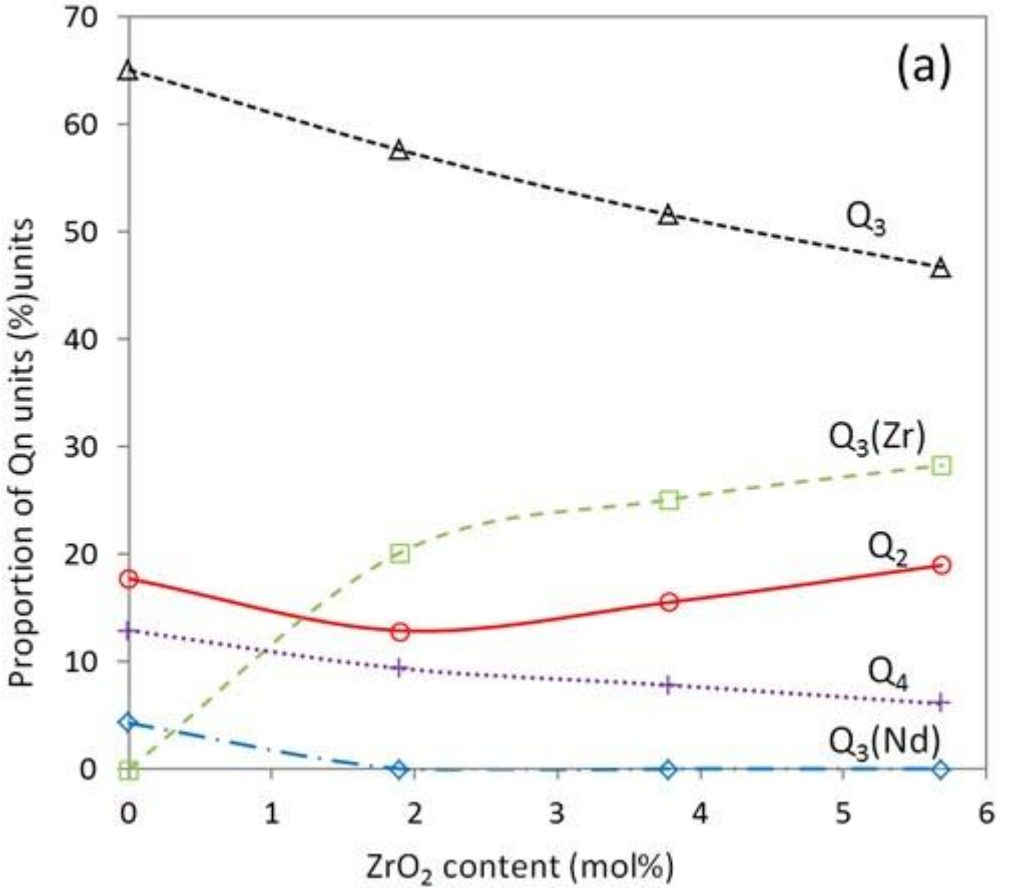
(a)
Proportion of Qn units (%)units
70
60
50
40
30
20
10
0
0
1
2
3
4
5
6
ZrO2 content (mol%)
Q3
Q3(Zr)
Q2
Q4
Q3(Nd)

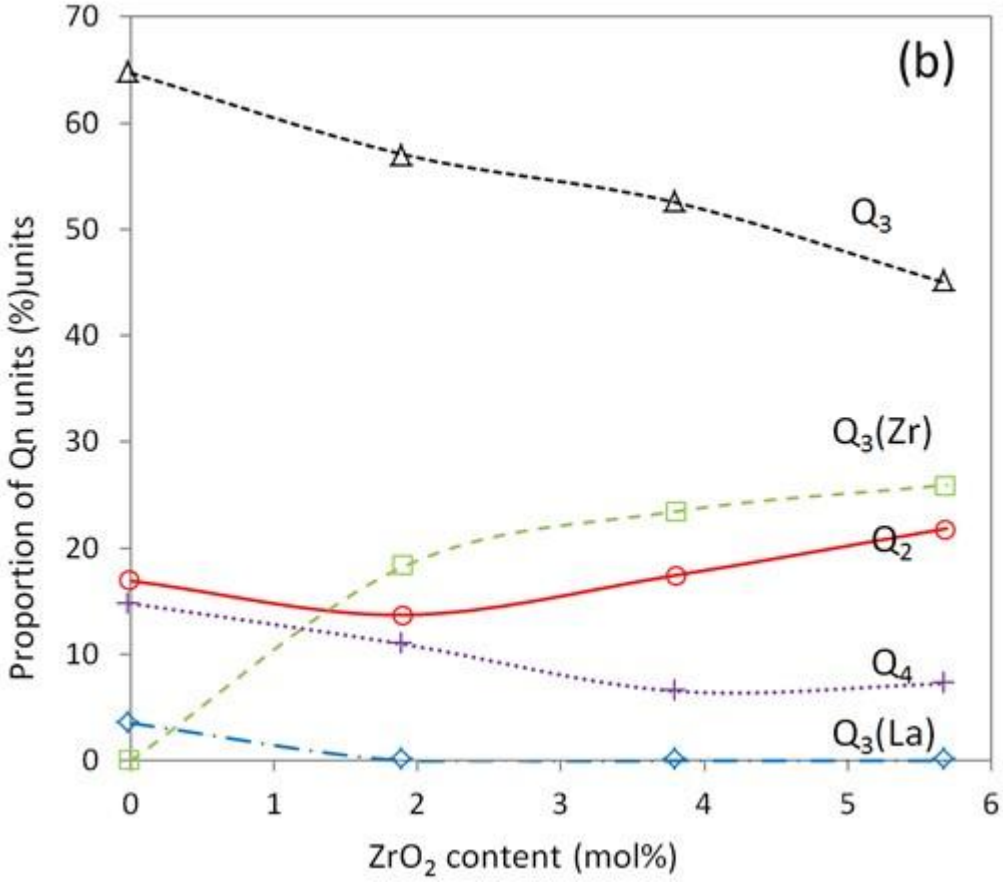
(b)
Proportion of Qn units (%)units
70
60
50
40
30
20
10
0
0
1
2
3
4
5
6
ZrO2 content (mol%)
Q3
Q3(Zr)
Q2
Q4
Q3(La)

Figure 7

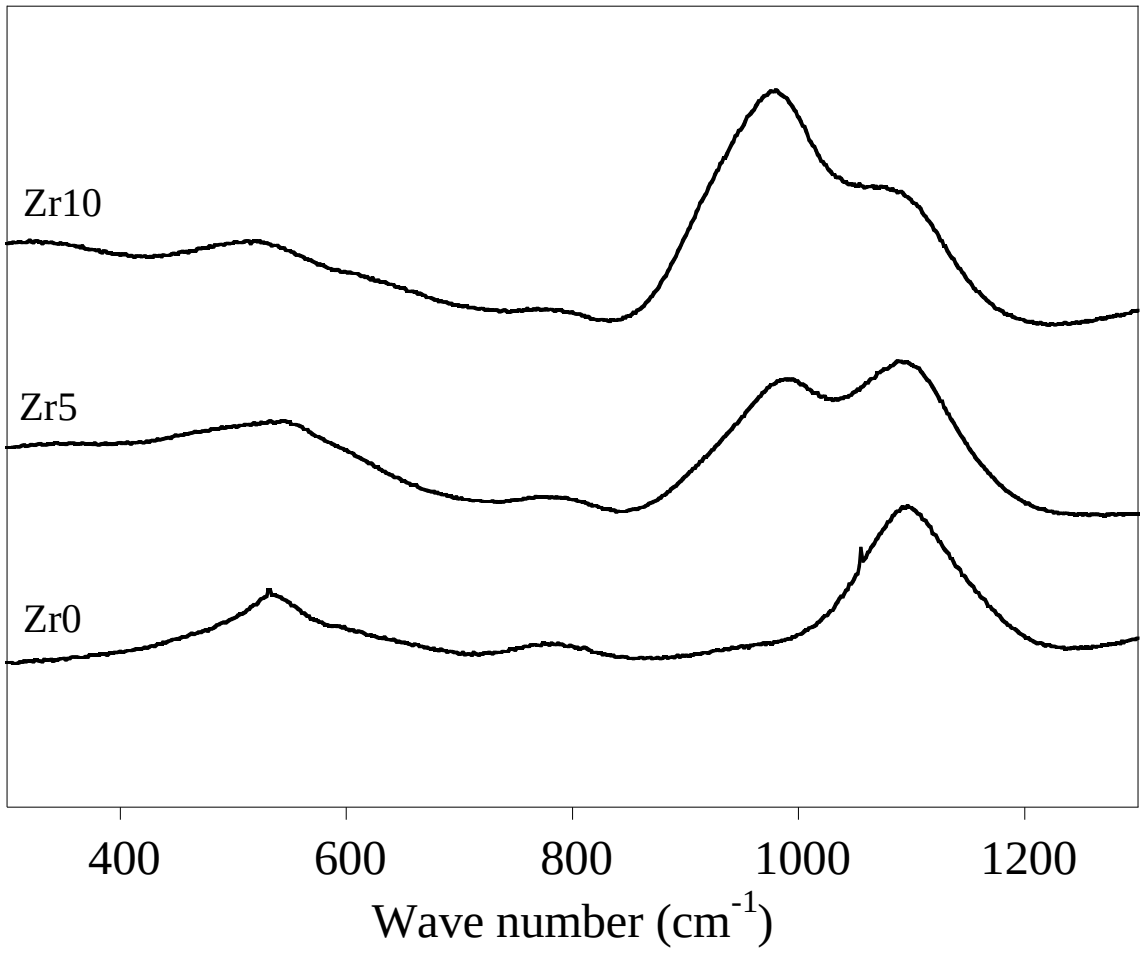

Figure 8

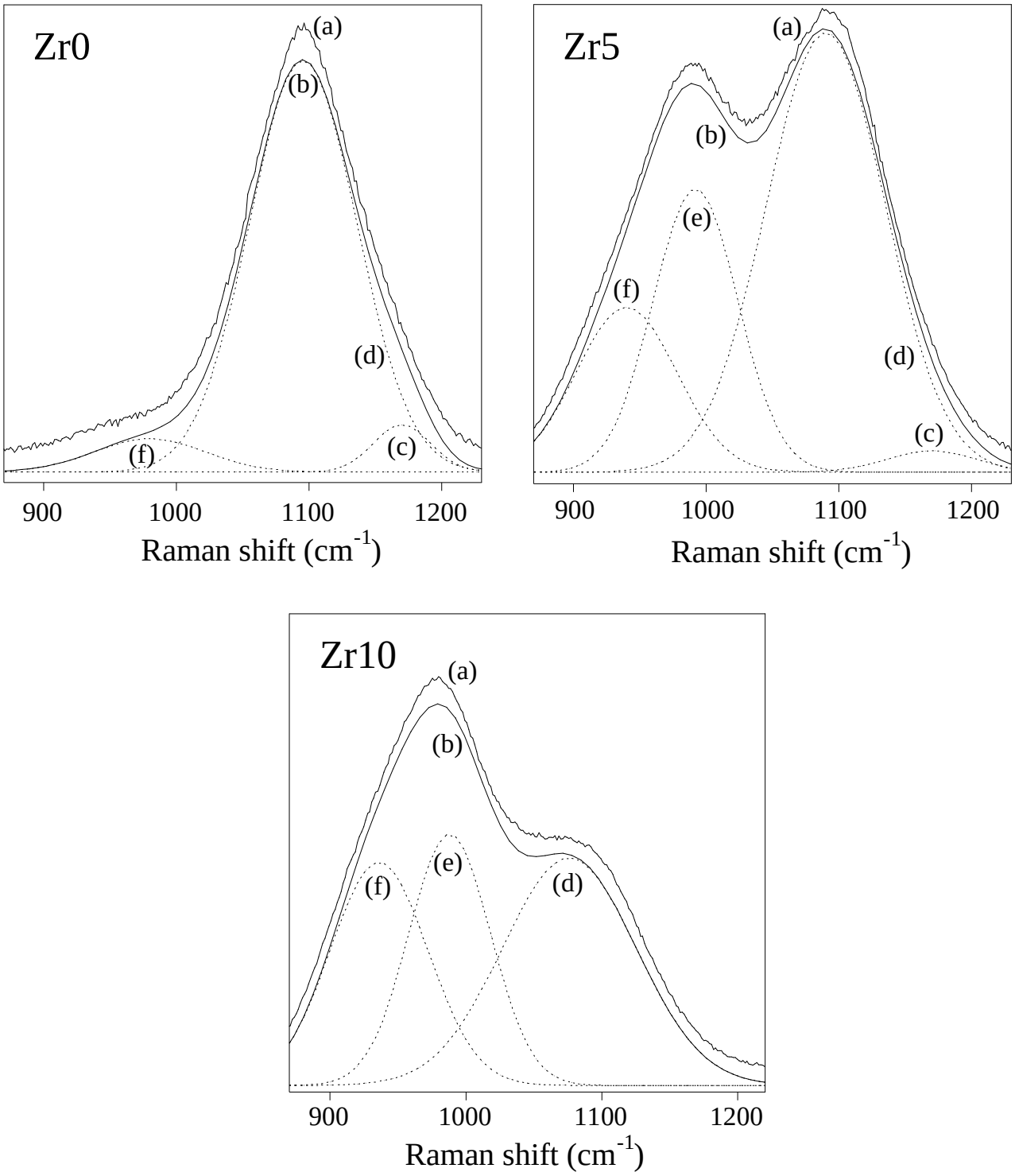
Zr0
(a)
(b)
(d)
(f)
(c)
900
1000
1100
1200
Raman shift (cm-1)
Zr5
(a)
(b)
(e)
(f)
(d)
(c)
900
1000
1100
1200
Raman shift (cm-1)
Zr10
(a)
(b)
(e)
(f)
(d)
900
1000
1100
1200
Raman shift (cm-1)

Figure 9

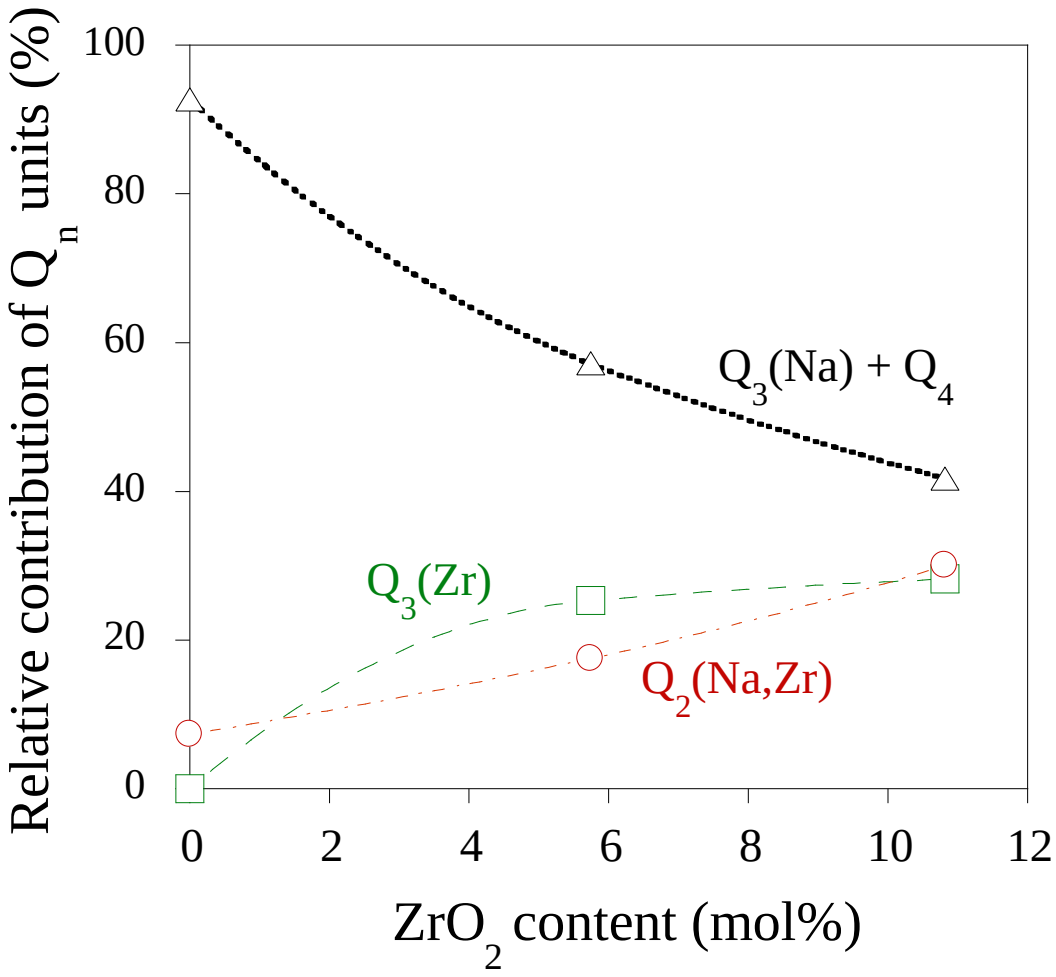
Relative contribution of Q_n units (%)
100
80
60
40
20
0
0
2
4
6
8
10
12
ZrO_2 content (mol%)
Q_3(Na) + Q_4
Q_3(Zr)
Q_2(Na,Zr)

Figure 10

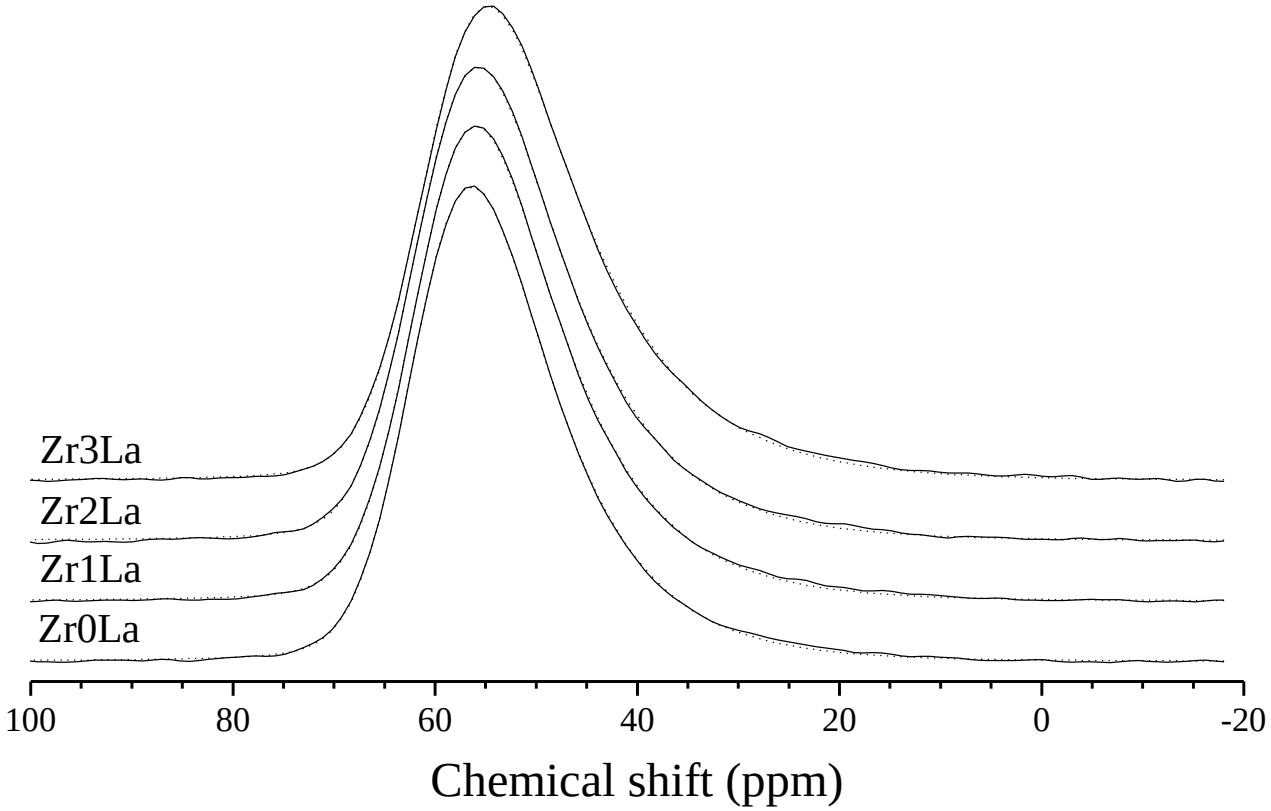
Zr3La
Zr2La
Zr1La
Zr0La
100
80
60
40
20
0
-20
Chemical shift (ppm)

Figure 11

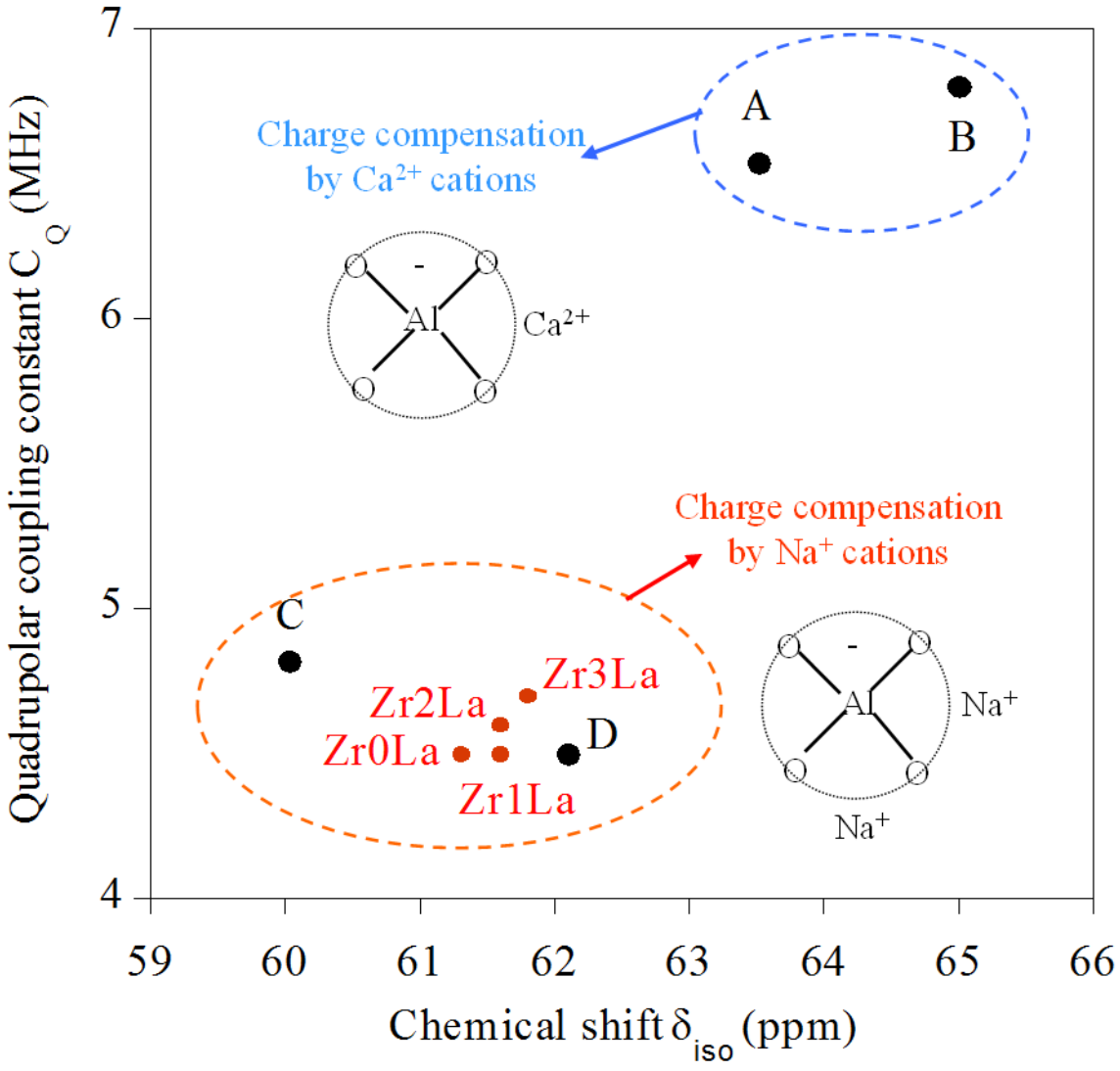
Quadrupolar coupling constant C_Q (MHz)
7
6
5
4
59
60
61
62
63
64
65
66
Chemical shift δ_{iso} (ppm)
Charge compensation by Ca^{2+} cations
A
B
Al
Ca^{2+}
Charge compensation by Na^+ cations
C
Zr3La
Zr2La
Zr0La
D
Zr1La
Al
Na^+
Na^+

Figure 12

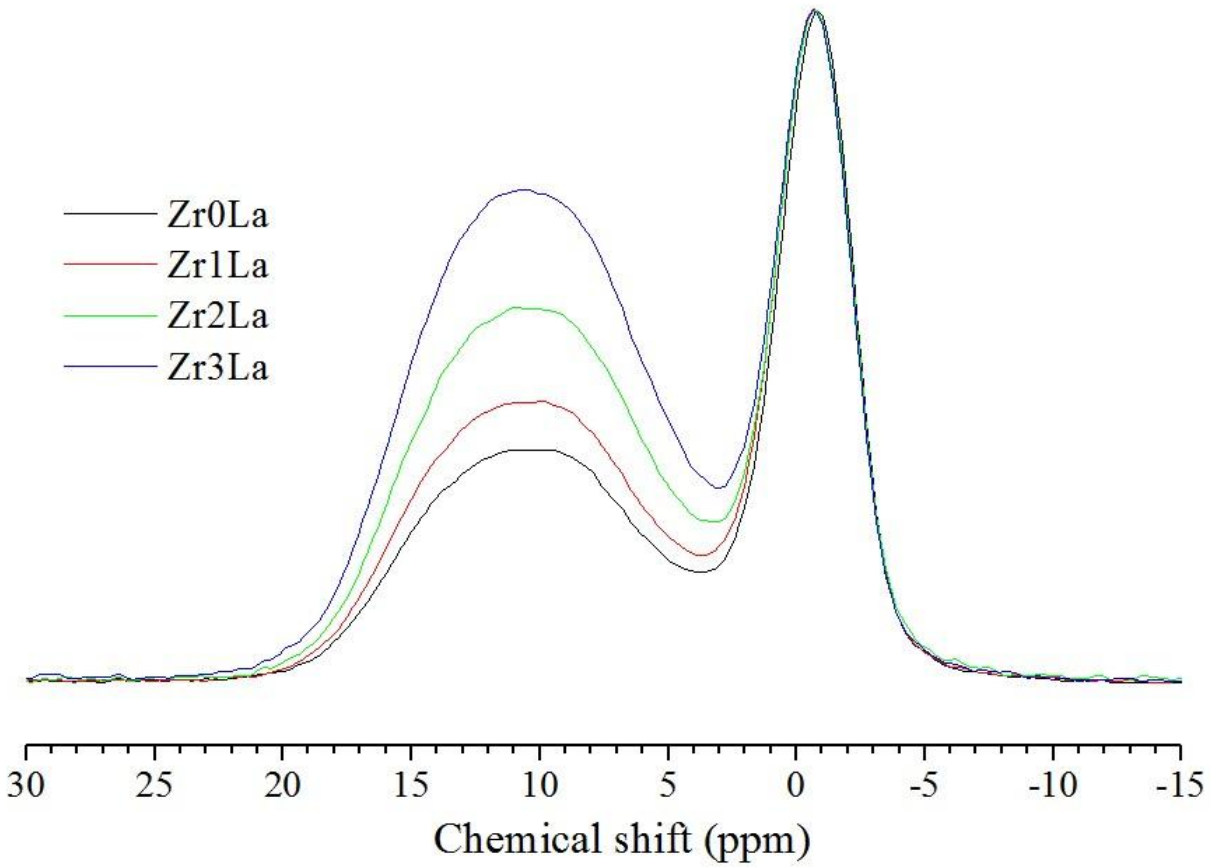
Zr0La
Zr1La
Zr2La
Zr3La
30
25
20
15
10
5
0
-5
-10
-15
Chemical shift (ppm)

Figure 13

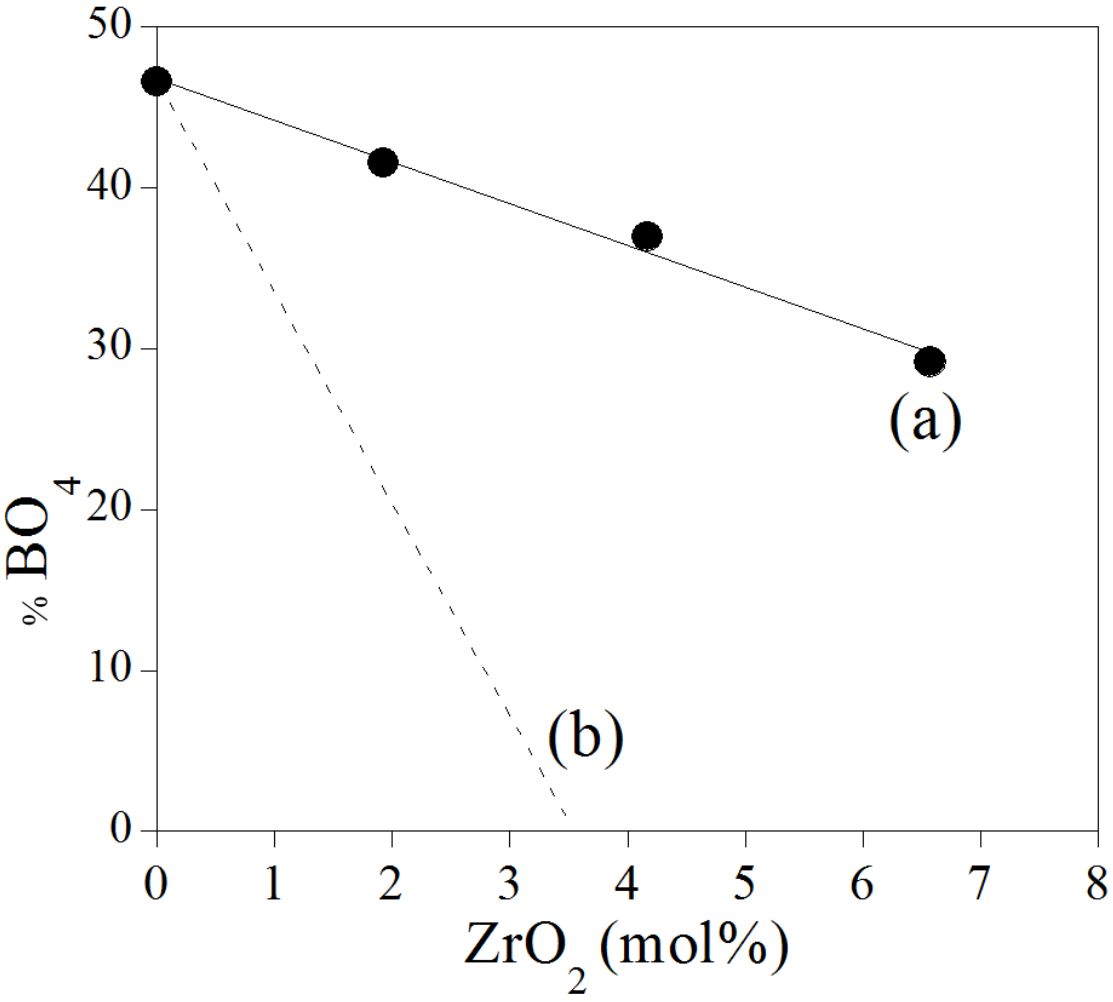

Figure 14

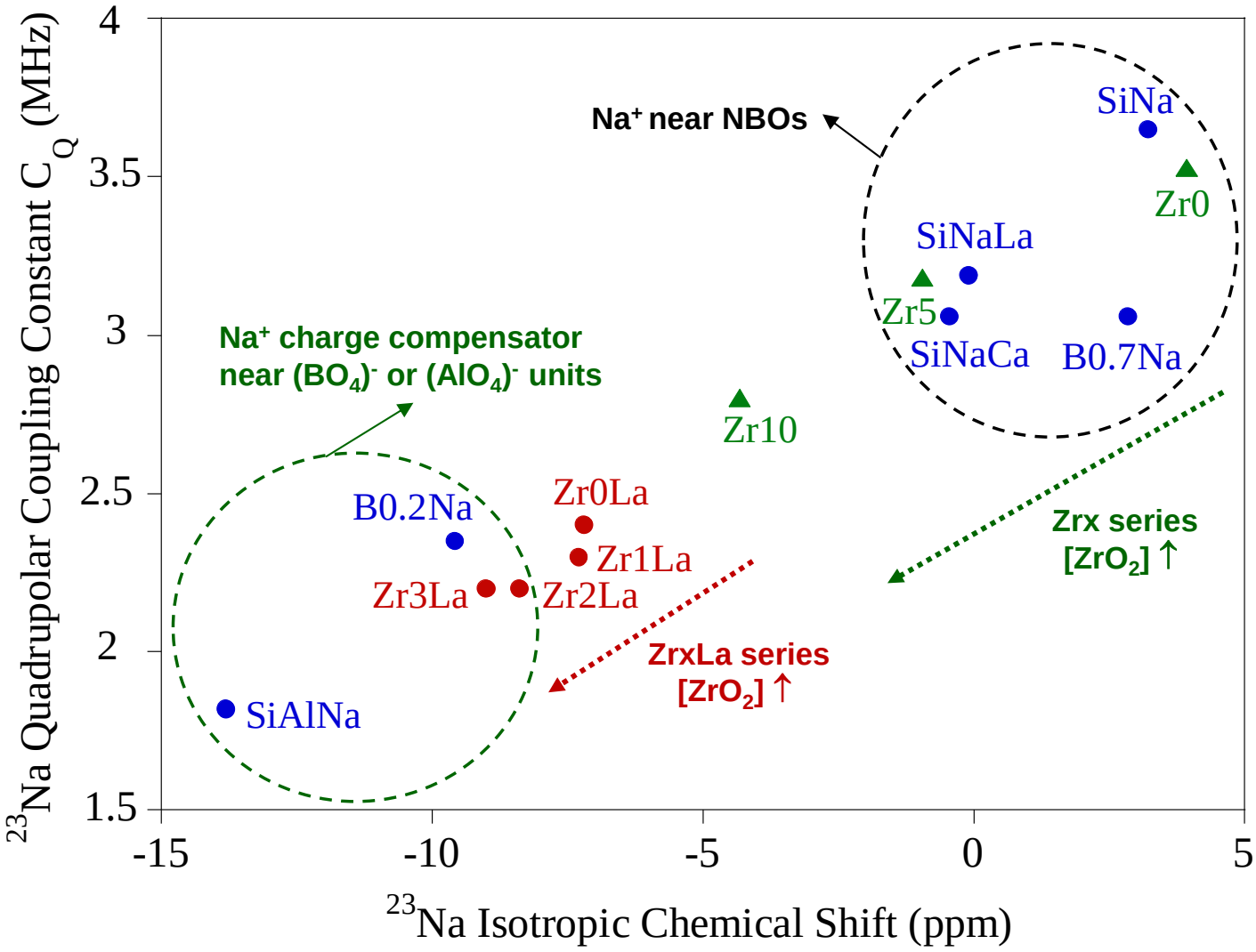
Na+ near NBOs
SiNa
Zr0
SiNaLa
Zr5
SiNaCa
B0.7Na
Na+ charge compensator
near (BO4)- or (AlO4)- units
Zr10
B0.2Na
Zr0La
Zr1La
Zr3La
Zr2La
SiAlNa
Zrx series
[ZrO2] ↑
ZrxLa series
[ZrO2] ↑
23Na Quadrupolar Coupling Constant CQ (MHz)
23Na Isotropic Chemical Shift (ppm)
4
3.5
3
2.5
2
1.5
-15
-10
-5
0
5

Figure 15

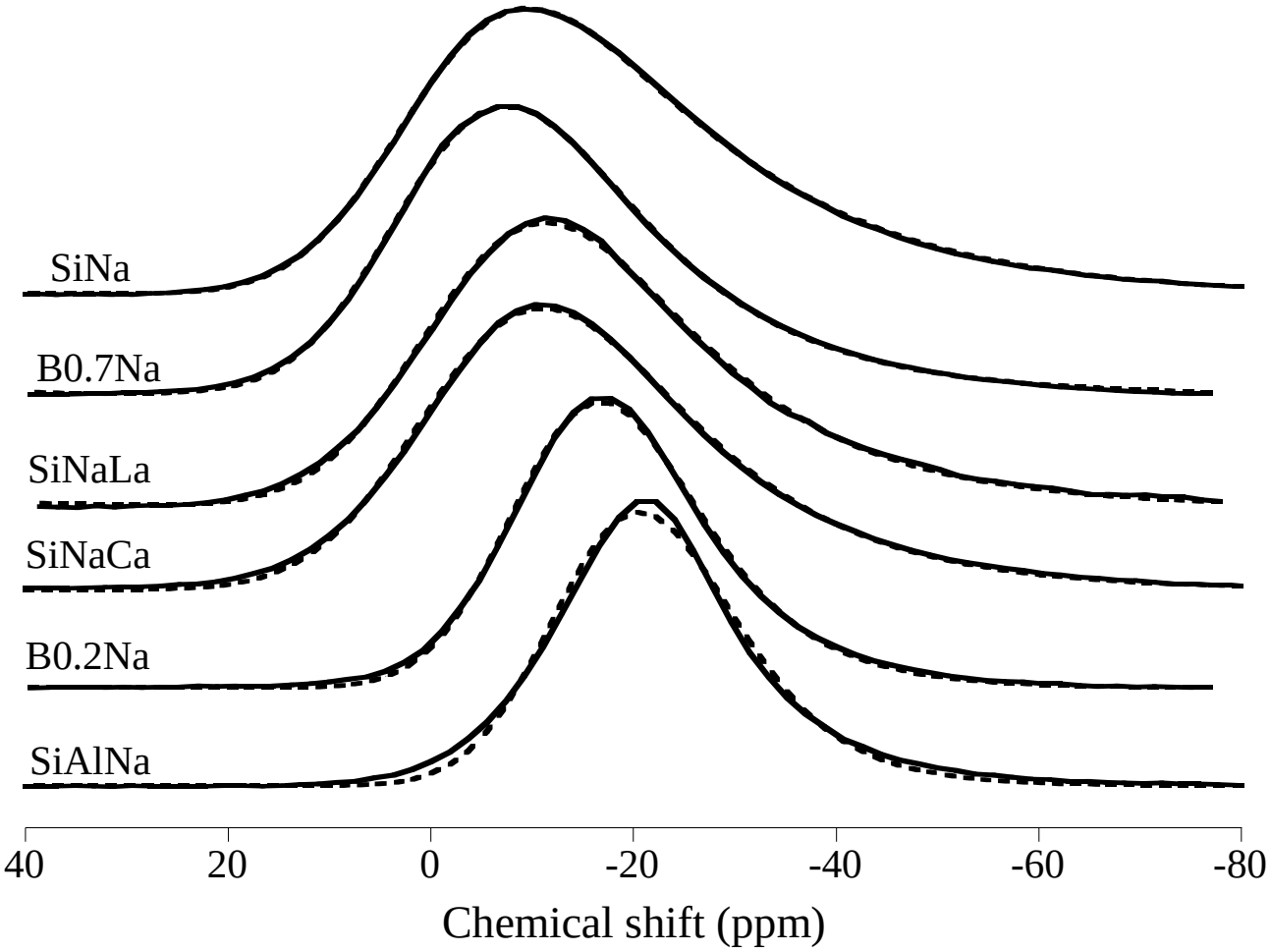
SiNa
B0.7Na
SiNaLa
SiNaCa
B0.2Na
SiAlNa
40
20
0
-20
-40
-60
-80
Chemical shift (ppm)

Figure 16

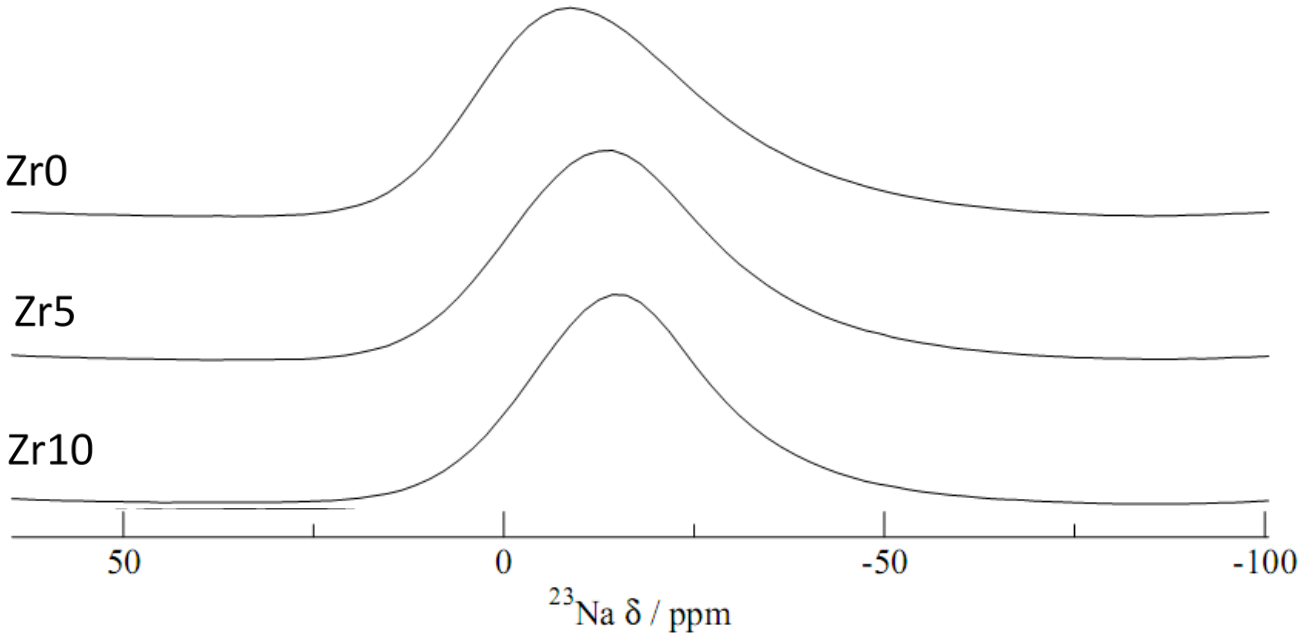

Figure 17

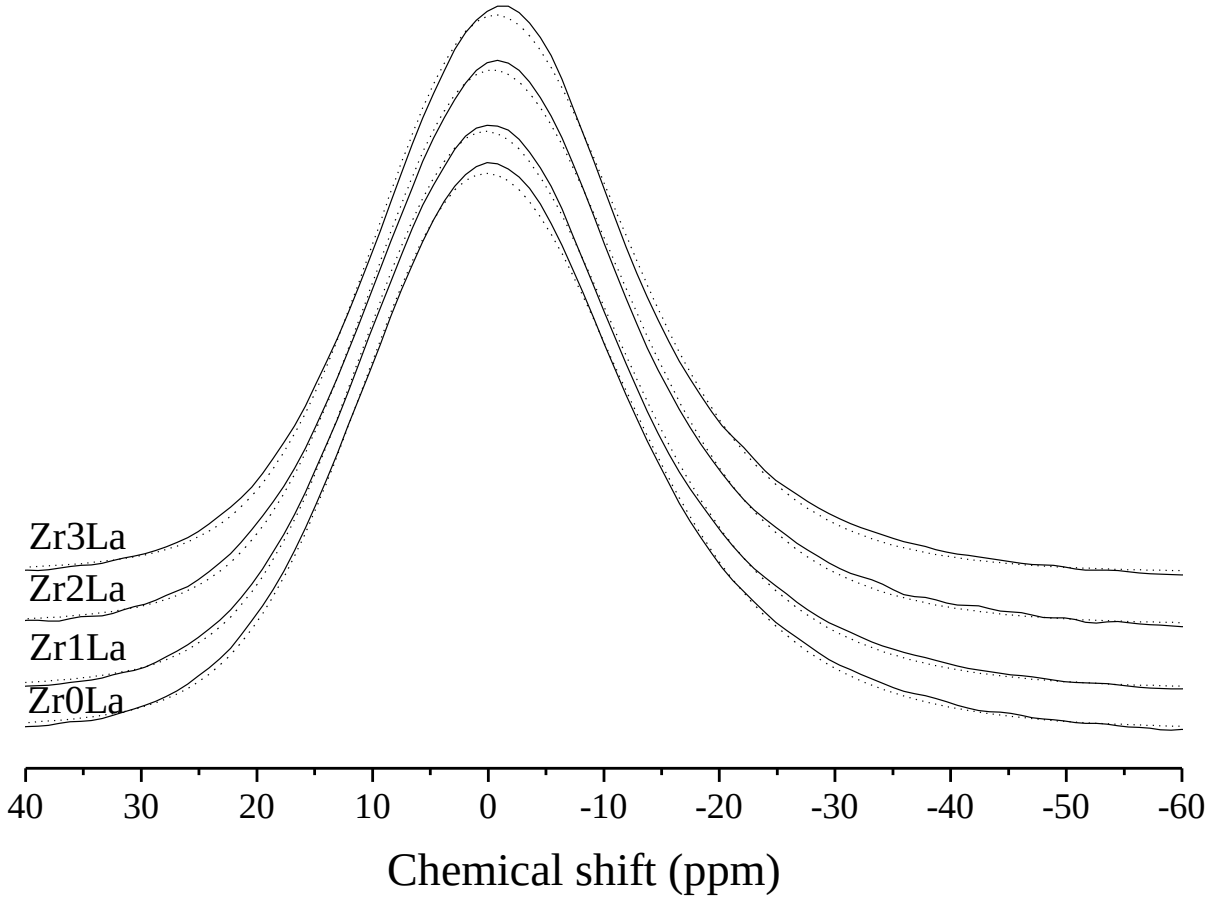
Zr3La
Zr2La
Zr1La
Zr0La
40
30
20
10
0
-10
-20
-30
-40
-50
-60
Chemical shift (ppm)

Figure 18

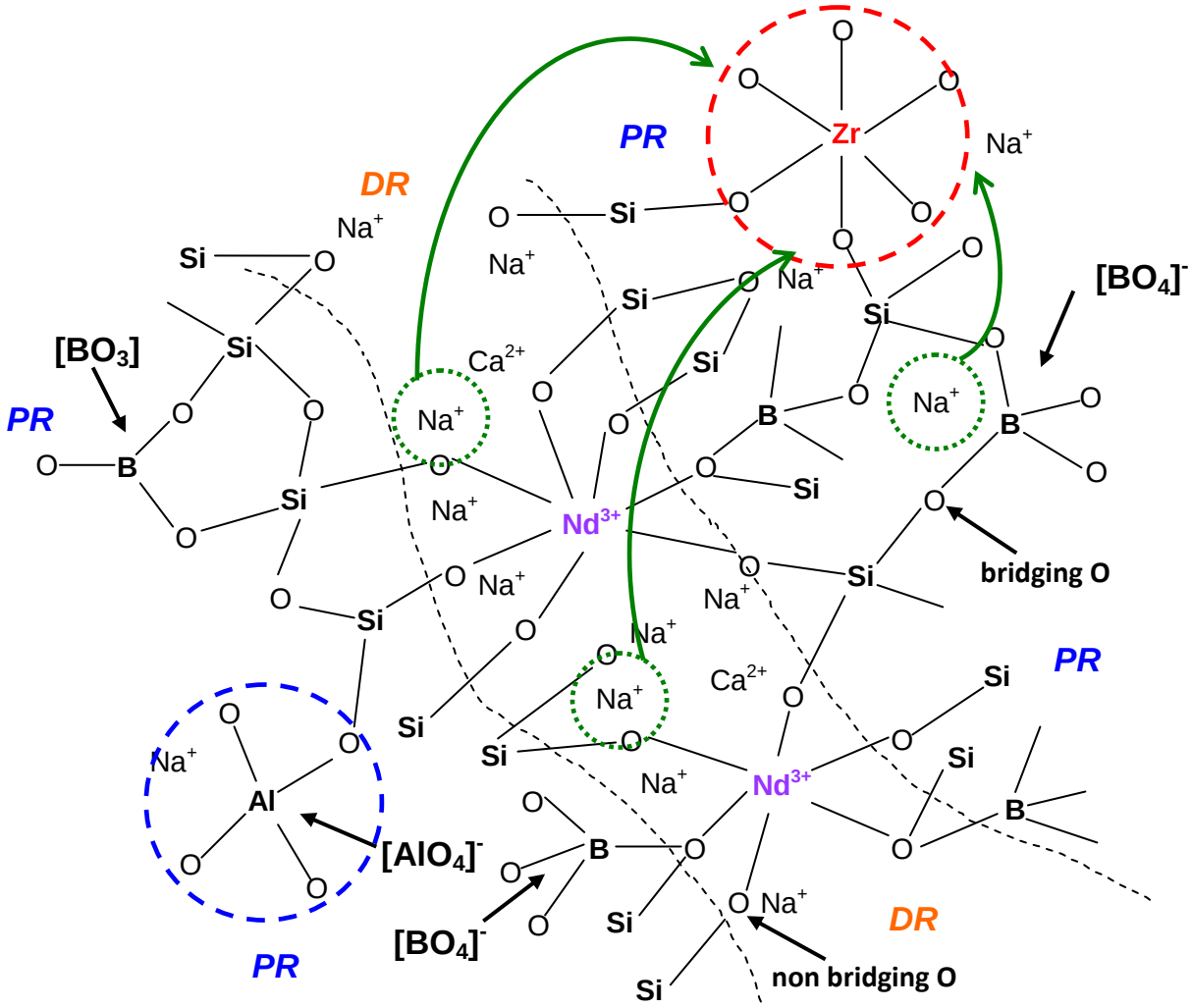
PR
DR
[BO3]
[BO4]-
[AlO4]-
bridging O
non bridging O
Zr
Nd3+
Ca2+
Na+
Si
B
Al
O

Figure 19

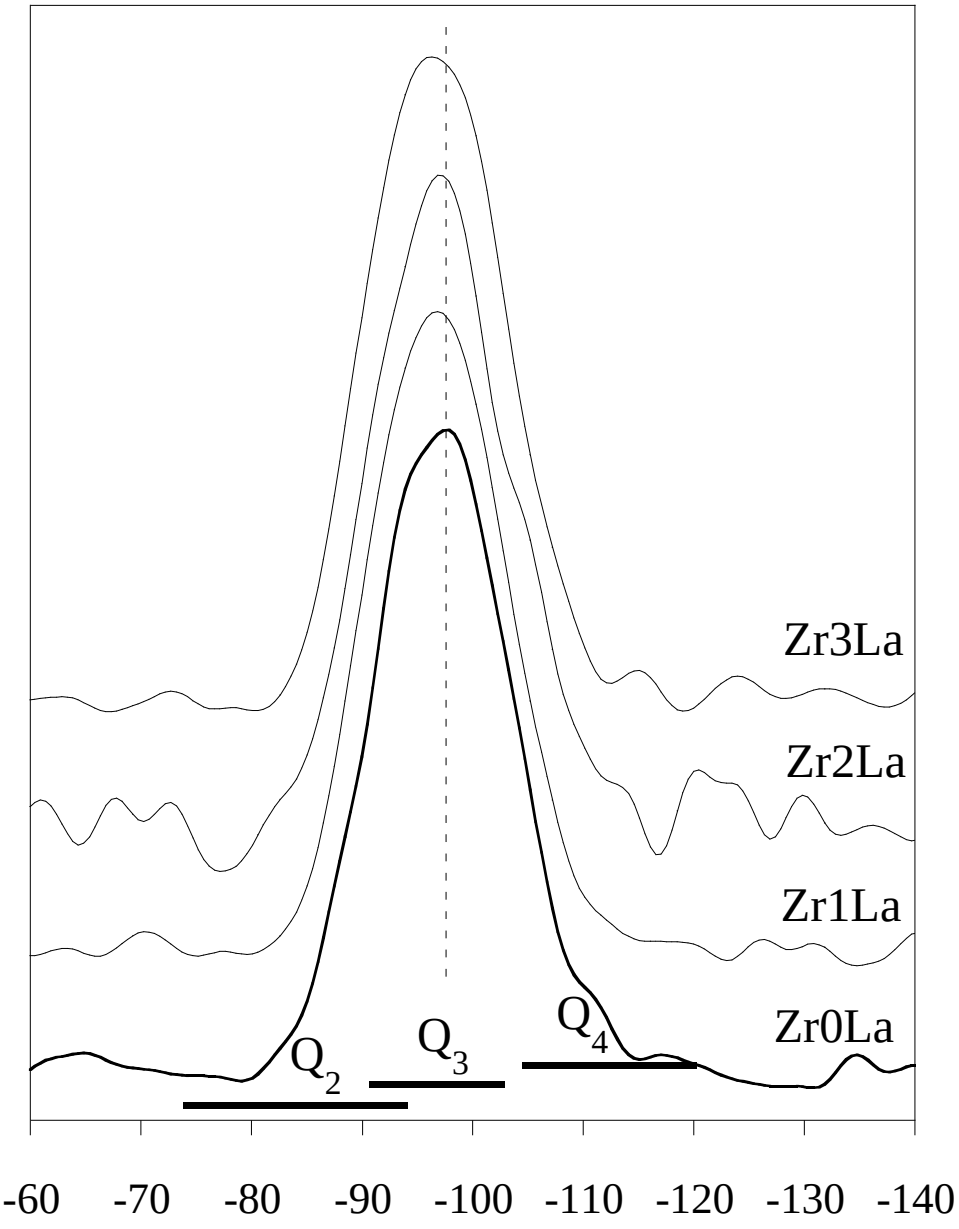
Zr3La
Zr2La
Zr1La
Zr0La
Q2
Q3
Q4
-60
-70
-80
-90
-100
-110
-120
-130
-140
Chemical shift (ppm)

Figure 20

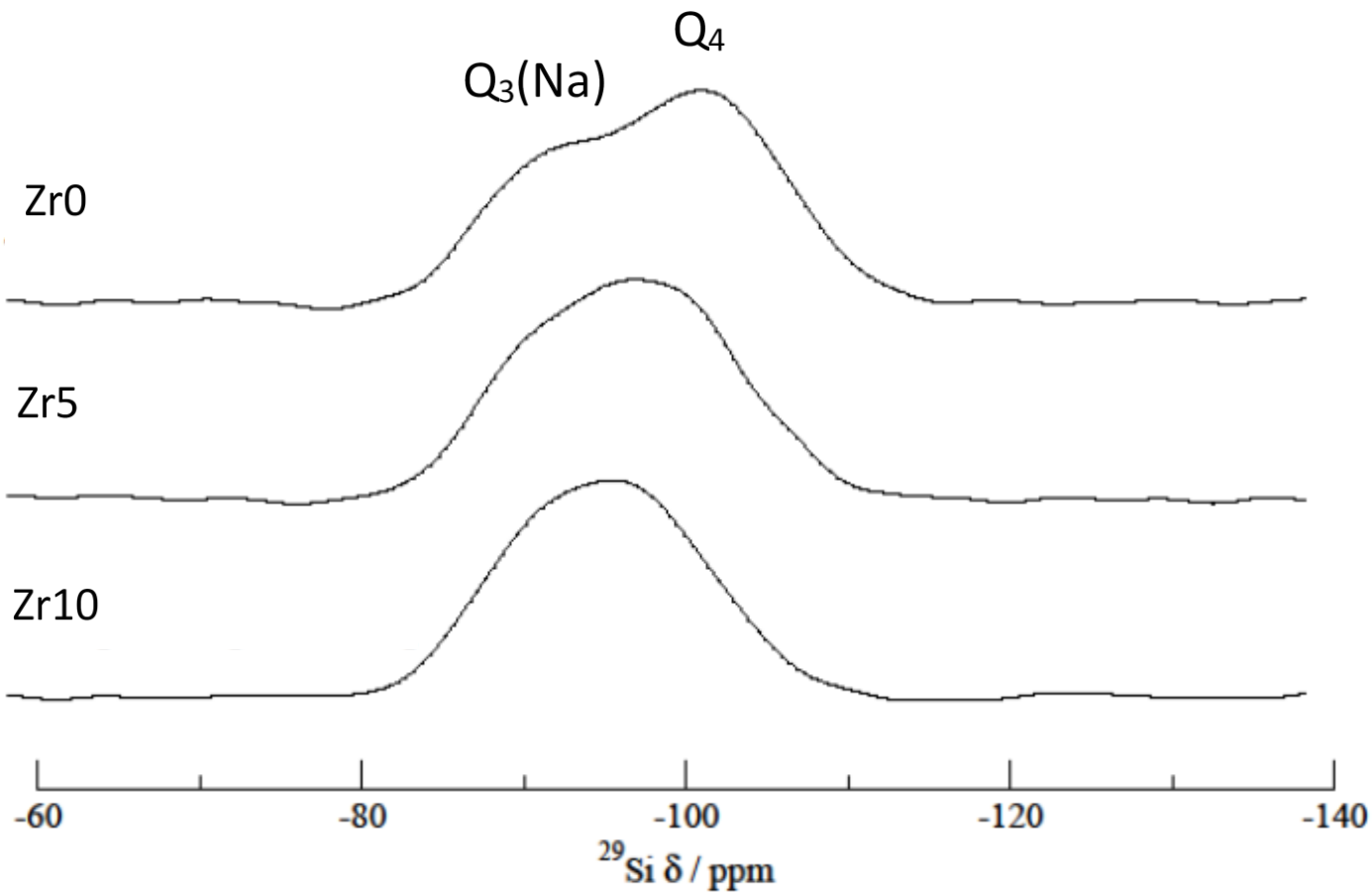

References

[1] R.G. Simhan, Chemical durability of ZrO_2 containing glasses, J. Non-Cryst. Solids 54 (1983) 335-343.

[2] C. Cailleteau, F. Angeli, F. Devreux, S. Gin, J. Jestin, P. Jollivet, O. Spalla, Insight into silicate glass corrosion, Nature Mater. 7 (2008) 978-983.

[3] B. Bergeron, L. Galoisy, P. Jollivet, F. Angeli, T. Charpentier, G. Calas, S. Gin, First investigations of the influence of IVB elements (Ti, Zr, and Hf) on the chemical durability of soda-lime borosilicate glasses, J. Non-Cryst. Solids 356 (2010) 2315-2322.

[4] M. H. Chopinet, Glass fibers resistant to basic media and their applications to reinforcing of cement, US patent n° 4,835,122 (1989).

[5] V. T. Ylmaz, E. E. Lachowski, F. P. Glasser. Chemical and microstructural changes at alkali-resistant glass fiber-cement interfaces, J. Amer. Ceram. Soc. 74 (1991) 3054-3060.

[6] O. Dargaud, G. Calas, L. Cormier, L. Galoisy, C. Jousseaume, G. Querel, M. Newville, In situ study of nucleation of zirconia in an $MgO–Al_2O_3–SiO_2$ glass, J. Amer. Ceram. Soc. 93 (2010) 342-344.

[7] O. Dargaud, L. Cormier, N. Menguy, L. Galoisy, G. Calas, S. Papin, G. Querel, L. Olivi, Structural role of Zr^{4+} as a nucleating agent in a $MgO–Al_2O_3–SiO_2$ glass-ceramics: A combined XAS and HRTEM approach, J. Non-Cryst. Solids 356 (2010) 2928-2934.

[8] O. Dargaud, L. Cormier, N. Menguy, G. Patriarche, G. Calas, Mesoscopic scale description of nucleation processes in glasses, Appl. Phys. Lett. 99 (2011) 021904.

[9] L. Cormier, B. Cochain, A. Dugué, O. Dargaud, Transition elements and nucleation in glasses using X-ray absorption spectroscopy, Int. J. Appl. Glass Sci. 5 (2014) 126-135.

[10] L. Cormier, O. Dargaud, G. Calas, C. Jousseaume, S. Papin, N. Trcera, A. Cognigni, Zr environment and nucleation role in aluminosilicate glasses, Mater. Chem. Phys. 152 (2015) 41-47.

[11] G. H. Beall, L. R. Pinckney, Nanophase glass-ceramics, J. Am. Ceram. Soc. 82 (1999) 5-16.

[12] T. Höche, C. Patzig, T. Gemming, R. Wurth, C. Rüssel, I. Avramov, Temporal evolution of diffusion barriers surrounding $ZrTiO_4$ nuclei in lithia aluminosilicate glass-ceramics, Cryst. Growth Des. 12 (2012) 1556-1163.

[13] M. Chavoutier, D. Caurant , O. Majérus, R. Boulesteix, P. Loiseau, C. Jousseaume, E. Brunet, E. Lecomte, Effect of TiO_2 content on the crystallization and the color of (ZrO_2-TiO_2)-doped Li_2O-Al_2O_3-SiO_2 glasses, J. Non Cryst. Solids 384 (2014) 15-24.

[14] P. Riello, P. Canton, N. Comelato, S. Polizzi, M. Verità, G. Fagherazzi, H. Hofmeister, S. Hopfe, Nucleation and crystallization behavior of glass-ceramic materials in the Li_2O–Al_2O_3–SiO_2 system of interest for their transparency properties, J. Non-Cryst. Solids 288 (2001) 127-139.

[15] P. Loiseau, D. Caurant, O. Majérus, N. Baffier, C. Fillet, Crystallization study of (TiO_2, ZrO_2)-rich SiO_2-Al_2O_3-CaO glasses. Part I: Preparation and characterization of zirconolite-based glass-ceramics, J. Mater. Sci. 38 (2003) 843-852.

[16] J. Lucas, Fluoride glasses, J. Mater. Sci. 24 (1989) 1-13.

[17] D. Caurant, P. Loiseau, O. Majérus, V. Aubin-Chevaldonnet, I. Bardez, A. Quintas, Glasses, Glass-Ceramics and Ceramics for Immobilization of Highly Radioactive Nuclear Wastes, Nova Science Publishers, Hauppauge NY (2009).

[18] R. Do Quang, V. Petitjean, F. Hollebecque, O. Pinet, T. Flament, A. Prod'homme, in: WM'03 conference (Waste Management), February 23-27, 2003, Tucson, AZ Conference, http://www.wmsym.org/archives/2003/pdfs/92.pdf.

[19] R. Guillaumont, Éléments chimiques à considérer dans l'aval du cycle nucléaire, C. R. Chimie 7 (2004) 1129-1134.

[20] F. Angeli, T. Charpentier, M. Gaillard, P. Jollivet, Influence of zirconium of pristine and and leached soda-lime borosilicate glasses: Towards a quantitative approach by ^{17}O MQMAS NMR, J. Non-Cryst. Solids 354 (2008) 3713-3722.

[21] F. Angeli, M. Gaillard, P. Jollivet, T. Charpentier, Influence of glass composition and alteration solution on leached glass structure: A solid-state NMR investigation, Geochim. Cosmochim. Acta 70 (2006) 2577-2590.

[22] E. Pèlegrin, G. Calas, P. Ildefonse, P. Jollivet, L. Galoisy, Structural evolution of glass surface during alteration: Application to nuclear waste glasses, J. Non-Cryst. Solids 356, (2001) 2497-2508.

[23] I. Bardez, D. Caurant, J.L. Dussossoy, P. Loiseau, C. Gervais, F. Ribot, D.R. Neuville, N. Baffier, C. Fillet, Matrices envisaged for the immobilization of concentrated nuclear waste solutions, Nucl. Sci. Eng. 153 (2006) 272-284.

[24] J-M. Gras, R. Do Quang, H. Masson, T. Lieven, C. Ferry, C. Poinssot, Michel Debes, J-M. Delbecq, Perspectives on the closed fuel cycle – Implications for high-level waste matrices, J. Nucl. Mater. 362 (2007) 383-394.

[25] C. M. Jantzen, in Handbook of advanced radioactive waste conditioning technologies, Woodhead Publishing Limited 230 (2011).

[26] N. Chouard, D. Caurant, O. Majérus, J.-L. Dussossoy, A. Ledieu, S. Peuget, R. Baddour-Hadjean, J.-P. Pereira-Ramos, Effect of neodymium oxide on the solubility of MoO_3 in an aluminoborosilicate glass, J. Non-Cryst. Solids 357 (2011) 2752-2762.

[27] N. Chouard, D. Caurant , O. Majérus, N. Guezi-Hasni, J-L. Dussossoy, R. Baddour Hadjean, J-P. Pereira-Ramos, Thermal stability of SiO_2-B_2O_3-Al_2O_3-Na_2O-CaO glasses with high Nd_2O_3 and MoO_3 concentrations, J. Alloys Compd. 671 (2016) 84-99.

[28] J. V. Crum, L. Turo, B. Riley, M. Tang, A. Kossoy, Multi-Phase Glass-Ceramics as a Waste Form for Combined Fission Products: Alkalis, Alkaline Earths, Lanthanides, and Transition Metals, J. Am. Ceram. Soc. 95 (2012) 1297-1303.

[29] I. Bardez, D. Caurant, P. Loiseau, J. L. Dussossoy, C. Gervais, F. Ribot, D. R. Neuvilleand, N. Baffier, Structural characterization of rare earth rich glasses for nuclear waste immobilization, Phys. Chem. Glasses 46 (2005) 320-329.

[30] O. Majérus, D. Caurant, A. Quintas, J.-L. Dussossoy, I. Bardez, P. Loiseau, Effect of boron oxide addition on the Nd^{3+} environment in a Nd-rich soda-lime aluminoborosilicate glass, J. Non-Cryst. Solids 357 (2011) 2744-2751.

[31] A. Quintas, D. Caurant, O. Majérus, J.-L. Dussossoy, T. Charpentier, Effect of changing the rare earth cation type on the structure and crystallization behavior of an aluminoborosilicate glass, Phys. Chem. Glasses: Eur. J. Glass Sci. Technol. B, 49 (2008) 192-197.

[32] A. Quintas, T. Charpentier, O. Majérus, D. Caurant, J. L. Dussossoy, P. Vermaut, NMR study of a rare-earth aluminoborosilicate glass with CaO to Na_2O ratio, Appl. Magn. Reson. 32 (2007) 613-634.

[33] A. Quintas, D. Caurant, O. Majérus, T. Charpentier, J-L. Dussossoy, Effect of compositionnal variations on charge compensation of AlO_4 and BO_4 entities and on crystallization tendency of a rare-earth-rich aluminoborosilicate glass, Mater. Res. Bull. 44 (2009) 1895-1898.

[34] W. J. Weber, Radiation-damage in a rare-earth silicate with the apatite structure, J. Am. Ceram. Soc. 65 (1982) 544-548.

[35] A. Kidari, M. Magnin, R. Caraballo, M. Tribet, F. Doreau, S. Peuget, J-L. Dussossoy, I. Bardez-Giboire, C. Jégou, Solubility and partitioning of minor-actinides and lanthanides in alumino-borosilicate nuclear glass, Procedia Chem. 7 (2012) 554-558.

[36] A. Quintas, D. Caurant, O. Majérus, P. Loiseau, T. Charpentier, J-L. Dussossoy, ZrO_2 addition in soda-lime aluminoborosilicate glasses containing rare earths: Impact on rare earths environment and crystallization, J. Alloys Compd. (submitted)

[37] A. J. Conelly, N. C. Hyatt, K. P. Travis, R. J. Hand, E. R. Madrell, R.J.Short, The structural role of Zr within alkali borosilicate glasses for nuclear waste immobilisation, J. Non-Cryst. Solids 357 (2011) 1647-1656.

[38] D. A. McKeown, I. S. Muller, A. C. Buechele, I. L. Pegg, X-ray absorption studies of the local environment of Zr in high-zirconia borosilicate glasses, J. Non-Cryst. Solids 258 (1999) 98-109.

[39] F. Farges, C. W. Ponader, G. E. Brown, Structural environments of incompatible elements in silicate glass/melt systems: I. Zirconium at trace levels, Geochim. Cosmochim. Acta 55 (1991) 1563-1574.

[40] L. Galoisy, E. Pélegrin, M-A. Arrio, P. Ildefonse, G. Calas, D. Ghaleb, C. Fillet, F. Pacaud, Evidence for 6-coordinated zirconium in inactive nuclear waste glasses, J. Am. Ceram. Soc. 82 (1999) 2219-2224.

[41] G. Ferlat, L. Cormier, M. H. Thibault, L. Galoisy, G. Calas, J. M. Delaye, D. Ghaleb, Evidence for symmetric cationic sites in zirconium-bearing oxide glasses, Phys. Rev. B 73 (2006) 214207.

[42] N. E. Brese, M. O'Keefe, Bond-valence parameters for solids, Acta Cryst. B 47 (1991) 192-197.

[43] G. E. Brown, F. Farges, G. Calas, X-ray scattering and x-ray spectroscopy studies of silicate melts, Rev. Mineral. 32 (1995) 317-410.

[44] P. Jollivet, G. Calas, L. Galoisy, F. Angeli, B. Bergeron, S. Gin, M. P. Ruffoni, N. Trcera, An enhanced resolution of the structural environment of zirconium in borosilicate glasses, J. Non-Cryst. Solids 381 (2013) 40-47.

[45] F. Angeli, F. T. Charpentier, M. Gaillard P. Jollivet, Influence of zirconium on the structure of pristine and leached soda-lime borosilicate glasses: Towards a quantitative approach by ^{17}O MQMAS NMR, J. Non-Cryst. Solids 354 (2008) 3713-3722.

[46] F. Angeli, F. T. Charpentier, D. de Ligny, C. Cailleteau, Boron speciation in soda-lime borosilicate glasses containing zirconium, J. Am. Ceram. Soc. 93 (2010) 2693-2704.

[47] M. Arab, C. Cailleteau, F. Angeli, F. Devreux, L. Girard, O.Spalla, Aqueous alteration of five-oxide silicate glasses: Experimental approach and Monte Carlo modeling, J. Non-Cryst. Solids 354 (2008) 155-161.

[48] M. Lobanova, A. Ledieu, P. Barboux, F. Devreux, O. Spalla, J. Lambard, Effect of ZrO_2 on the glass durability, Mat. Res. Symp. Proc. 713 (2002) 571-579.

[49] O. Dargaud, L. Cormier, N. Menguy, G. Patriarche, Multi-scale structuration of glasses: Observations of phase separation and nanoscale heterogeneities in glasses by Z-contrast scanning electron transmission microscopy, J. Non-Cryst. Solids 358 (2012) 1257-1262.

[50] A. Quintas, O. Majérus, M. Lenoir, D. Caurant, K. Klementiev, A. Webb, Effect of alkali and alkaline-earth cations on the neodymium environment in a rare-earth rich aluminoborosilicate glass, J. Non-Cryst. Solids 354 (2008) 98-104.

[51] O. Majérus, D. Caurant, A. Quintas, J.L. Dussossoy, I. Bardez, P. Loiseau, Effect of boron oxide addition on the Nd^{3+} environment in a Nd-rich soda-lime aluminoborosilicate glass, J. Non-Cryst. Solids 357 (2011) 2744-2751.

[52] D. A. Long, Raman Spectroscopy, Ed. McGraw-Hill (New-York) (1977).

[53] M. Çelikbilek, A. Erçin Ersundu, S. Aydin, Glass formation and characterization studies in the TeO_2–WO_3–Na_2O system, J. Am. Ceram. Soc. 96 (2013) 1470-1476.

[54] J. G. Fisher, P. F. James, J. M. Parker, J. Non-Cryst. Solids 351 (2005) 623-631.

[55] S. Ghose, C. Wan, Zektzerite, $NaLiZrSi_6O_{15}$: a silicate with six-tetrahedral-repeat double chains, Am. Mineral. 63 (1978) 304-310.

[56] V. Dimitrov and T. Komatsu, Correlation between optical basicity and single bond strength of simple oxides and sodium containing oxide glasses, Phys. Chem. Glasses: Eur. J. Glass Sci. Technol. B 49 (2008) 33-40.

[57] J. A. Duffy, M. D. Ingram, Solvent properties of glass melts: Resemblance to aqueous solutions, C. R. Chimie 5 (2002) 797-804.

[58] D. A. McKeown, I. S. Muller, A. C. Buechele, I. L. Pegg, C.A. Kendziora, Structural characterization of high-zirconia borosilicate glasses using Raman spectroscopy, J. Non-Cryst. Solids 262 (2000) 126-134.

[59] B. C. Bunker, D.R. Tallant, R.J. Kirkpatrick, G.L. Turner, Nuclear magnetic resonance and Raman investigation of sodium borosilicate glass structures, Phys. Chem. Glasses 31 (1990) 30-40.

[60] D. Manara, A. Grandjean, D. R. Neuville, Advances in understanding the structure of borosilicate glasses: A Raman spectroscopy study, Am. Mineral. 94 (2009) 777-784.

[61] T. Schaller, J. F. Stebbins, M. C. Wilding, Cation clustering and formation of free oxide ions in sodium and potassium lanthanum silicate glasses: nuclear magnetic resonance and Raman spectroscopic findings, J. Non-Cryst. Solids 243 (1999) 146-157.

[62] A. J. G. Ellison, P. C. Hess, Raman study of potassium silicate glasses containing Rb^+, Sr^{2+}, Y^{3+} and Zr^{4+}: Implications for cation solution mechanisms in multicomponent silicate liquids, Geochim. Cosmochim. Acta 58 (1994) 1877-1887.

[63] E. Sokolova, F. C. Hawthorne, N.A. Ball, R. H. Mitchell, G. D. Ventura, Vlasovite $Na_2Zr(Si_4O_{11})$, from the Kipawa alkaline complex, Quebec Canada: crystal-structure refinement and infrared spectroscopy, Can. Mineral. 44 (2006) 1349-1356.

[64] RRUFF Project website database of Raman spectra, X-ray diffraction and chemistry data for minerals, http://rruff.info/vlasovite.

[65] S. W. Lee, R. A. Condrate, The infrared and Raman spectra of ZrO_2-SiO_2 glasses prepared by a sol-gel process, J. Mater. Sci. 23 (1988) 2951-2959.

[66] S. G. Fleet, The crystal structure of dalyite, Z. Kristall.121 (1965) 349-368.

[67] A. J. G. Ellison, P. C. Hess, Lanthanides in silicate glasses: A vibrational spectroscopic study, J. Geol. Res. 95 (1990) 15717-15726.

[68] L. Cormier, D. Ghaleb, J.-M. Delaye, G. Calas, Competition for charge compensation in borosilicate glasses: Wide-angle x-ray scattering and molecular dynamics calculations, Phys. Rev. B. 61 (2000) 14495.

[69] A. N. Cormack, J. Du, Molecular dynamics simulations of soda–lime–silicate glasses, J. Non-Cryst. Solids 293-295 (2001) 283-289.

[70] A. Bonamartini Corradi, V. Cannillo, M. Monia, C. Siligardi, Local and medium range structure of erbium containing glasses: A molecular dynamics study, J. Non-Cryst. Solids 354 (2008) 173-180.

[71] N. Ollier, T. Charpentier, B. Boizot, G. Wallez, D. Ghaleb, A Raman and MAS NMR study of mixed alkali Na–K and Na–Li aluminoborosilicate glasses, J. Non-Cryst. Solids 341 (2004) 26-34.

[72] A. Soleilhavoup, J.-M. Delaye, F. Angeli, D. Caurant, T. Charpentier, Contribution of first-principles calculations to multinuclear NMR analysis of borosilicate glasses, Magn. Reson. Chem. 48 (2010) S159-S170.

[73] E. Gambuzzi, T. Charpentier, M. C. Menziani, A. Pedone, Computational interpretation of ^{23}Na MQMAS NMR spectra: A comprehensive investigation of the Na environment in silicate glasses, Chem. Phys. Lett. 612 (2014) 56-61.

[74] K. J. D. MacKenzie, M. E. Smith, Multinuclear Solid-State NMR of Inorganic Materials, Pergamon Materials Series, Elsevier Science Ltd. (2002).

[75] F. Angeli, J. M. Delaye, T. Charpentier, J. C. Petit, D. Ghaleb, P. Faucon, Influence of glass chemical composition on the Na–O bond distance: a ^{23}Na 3Q-MAS NMR and molecular dynamics study, J. Non-Cryst. Solids 276 (2000) 132-144.

[76] J. F. Stebbins, Cation sites in mixed-alkali oxide glasses: correlations of NMR chemical shift data with site size and bond distance, Solid State Ionics 112 (1998) 137-141.

[77] G. Engelhardt, H. Koller, ^{29}Si NMR of inorganic solids, in NMR-Basic Principles and Progress, Vol. 31, Springer, (1994) 1-29.

[78] O. B. Lapina, D. F. Khabibulin, V. V. Terskikh, Multinuclear NMR study of silica fiberglass modified with zirconia, Solid State Nucl. Magn. Reson. 39 (2011) 47–57.

[79] T. Nanba, M. Nishimura and Y. Miura, A theoretical interpretation of the chemical shift of ^{29}Si NMR peaks in alkali borosilicate glasses, Geochim. Cosmochim Acta 68 (2004) 5103-5111.

[80] H. Maekawa, T. Maekawa, K. Kawamura, T. Yokokawa, The structural groups of alkali silicate glasses determined from ^{29}Si MAS-NMR, J. Non-Cryst. Solids 127 (1991) 53-64.

[81] P. Loiseau, D. Caurant, N. Baffier, K. Dardenne, J. Rothe, M. Denecke, S. Mangold, Structural characterization of Nd-doped calcium aluminosilicate glasses designed for the preparation of zirconolite ($CaZrTi_2O_7$)-based glass-ceramics, XXIst International

Congress on Glass, Abstract A42 (July 1-6, 2007 Strasbourg, France), http://hal.archives-ouvertes.fr/hal-00584146/fr/.

[82] C. Meneghini, S. Mobilio, L. Lusvarghi, F. Bondioli, A. M. Ferrari, T. Manfredini, C. Siligardi, The structure of ZrO_2 phases and devitrification processes in a Ca–Zr–Si–O-based glass ceramic: a combined a-XRD and XAS study, J. Appl. Cryst. 37 (2004) 890-900.

[83] RRUFF Project website database of Raman spectra, X-ray diffraction and chemistry data for minerals, http://rruff.info/zektzerite.

[84] G. N. Greaves, A. Fontaine, P. Lagarde, D. Raoux, S. J. Gurman, Local structure of silicate glasses, Nature 293 (1981) 611-616.

[85] G. N. Greaves, EXAFS and the structure of glass, J. Non-Cryst. Solids 71 (1985) 203-217.